

**MULTI-HAZARD SUSCEPTIBILITY MAP PRODUCTION
FOR URBAN PLANNING PURPOSES: ANKARA MAMAK
CASE**

**KENTSEL PLANLAMA AMAÇLI ÇOKLU DOĞAL
TEHLİKE DUYARLILIK HARİTASI ÜRETİMİ: ANKARA
MAMAK ÖRNEĞİ**

TUĞÇE YANAR

ASSOC.PROF.DR. SULTAN KOCAMAN GÖKÇEOĞLU

Submitted to

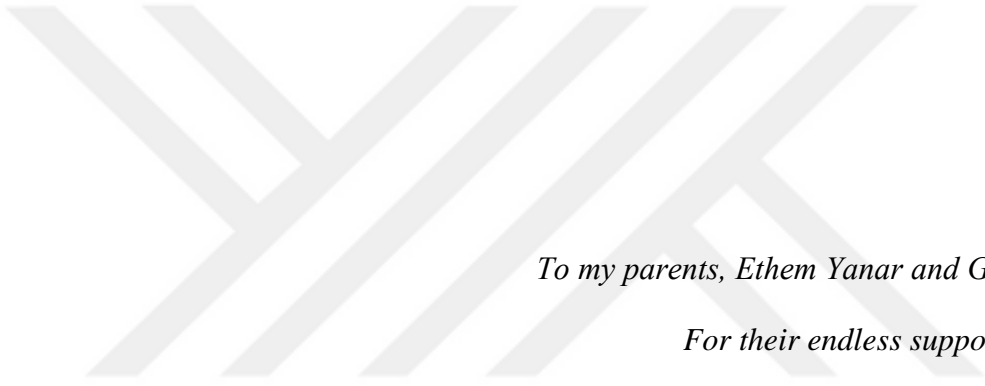
Graduate School of Science and Engineering of Hacettepe University

as a Partial Fulfillment to the Requirements

for the Award of the Degree Master of Science

in Geomatics Engineering

2020



To my parents, Ethem Yanar and Gönül Yanar

For their endless support and love.

ETHICS

In this thesis study, prepared in accordance with the spelling rules of Institute of Graduate Studies in Science of Hacettepe University.

I declare that

- all the information and documents have been obtained in the base of academic rule,
- all audio-visual and written information and results have been presented according to the rules of scientific ethics,
- in case of using other works, related studies have been cited in accordance with the scientific standards,
- all cited studies have been fully referenced,
- I did not do any distortion in the data set,
- and any part of this thesis has not been presented as another thesis study at this or any other university.

21 / 04 / 2020

T. Yanar

TUĞÇE YANAR

YAYINLANMA FİKRİ MÜLKİYET HAKLARI BEYANI

Enstitü tarafından onaylanan lisansüstü tezimin/raporumun tamamını veya herhangi bir kısmını, basılı (kağıt) ve elektronik formatta arşivleme ve aşağıda verilen koşullarla kullanıma açma iznini Hacettepe üniversitesine verdiğimi bildiririm. Bu izinle Üniversiteye verilen kullanım hakları dışındaki tüm fikri mülkiyet haklarım bende kalacak, tezimin tamamının ya da bir bölümünün gelecekteki çalışmalarda (makale, kitap, lisans ve patent vb.) kullanım hakları bana ait olacaktır.

Tezin kendi orijinal çalışmam olduğunu, başkalarının haklarını ihlal etmediğimi ve tezimin tek yetkili sahibi olduğumu beyan ve taahhüt ederim. Tezimde yer alan telif hakkı bulunan ve sahiplerinden yazılı izin alınarak kullanması zorunlu metinlerin yazılı izin alarak kullandığımı ve istenildiğinde suretlerini Üniversiteye teslim etmeyi taahhüt ederim.

Yükseköğretim Kurulu tarafından yayınlanan "*Lisansüstü Tezlerin Elektronik Ortamda Toplanması, Düzenlenmesi ve Erişime Açılmasına İlişkin Yönerge*" kapsamında tezim aşağıda belirtilen koşullar haricince YÖK Ulusal Tez Merkezi / H. Ü. Kütüphaneleri Açık Erişim Sisteminde erişime açılır.

- Enstitü / Fakülte yönetim kurulu kararı ile tezimin erişime açılması mezuniyet tarihimden itibaren 2 yıl ertelenmiştir.
- Enstitü / Fakülte yönetim kurulu gerekçeli kararı ile tezimin erişime açılması mezuniyet tarihimden itibaren ay ertelenmiştir.
- Tezim ile ilgili gizlilik kararı verilmiştir.

21. / 04 / 2020

T. Yanar

TUĞÇE YANAR

ABSTRACT

MULTI-HAZARD SUSCEPTIBILITY MAP PRODUCTION FOR URBAN PLANNING PURPOSES: ANKARA MAMAK CASE

Tuğçe YANAR

Master of Science, Department of Geomatics Engineering

Supervisor: Assoc. Prof. Dr. Sultan KOCAMAN GÖKÇEOĞLU

April 2020, 70 pages

Multiple hazards may affect urban areas and integration of susceptibility maps about natural hazards are required for proper site selection and urban planning. Likewise, geological and geotechnical parameters, development expenditures and the spatial pattern of existent social and technical infrastructure should be considered for this aim. Up-to-date land use land cover (LULC) maps and the natural hazard susceptibility maps based on this data can be acquired from high-resolution satellite sensors. In this thesis, landslide and flood hazard potential are considered for combined hazard susceptibility assessment to be used for an urban settlement, Mamak, which is currently developing for disaster management purposes. The flood susceptibility map of Ankara City was generated in a prior research with the Modified Analytical Hierarchical Process (M-AHP) method. The landslide susceptibility map was generated with the logistic regression method in this thesis. LULC map was obtained from Sentinel-2 images with the Random Forest method

as an image classification technique. The first and second topographic derivatives acquired by a digital terrain model (DTM) and lithology information produced by the General Directorate of Mineral Research and Explorations were employed for the generation of landslide susceptibility maps. A combined hazard susceptibility assessment was performed using the Mamdani Fuzzy algorithm and the outcomes were examined in the context of urban planning. According to the results, multi-hazard susceptibility assessment maps, which can be a base for city planning, can be created by combining a number of machine learning and expert-based learning methods.

Keywords: Multi-Hazard, Natural Hazard Susceptibility Map, Landslide, Flood, Urban Settlements, Random Forest, Logistic Regression, Mamdani Fuzzy Algorithm.

ÖZET

KENTSEL PLANLAMA AMAÇLI ÇOKLU DOĞAL TEHLİKE DUYARLILIK HARİTASI ÜRETİMİ: ANKARA MAMAK ÖRNEĞİ

Tuğçe YANAR

Yüksek Lisans, Geomatik Mühendisliği Bölümü

Tez Danışmanı: Doç. Dr. Sultan KOCAMAN GÖKÇEOĞLU

Nisan 2020, 70 sayfa

Kentsel alanlarda çoklu afet tehlikeleri bulunmaktadır ve uygun yer seçimi ve şehir planlaması için çoklu tehlike duyarlılık haritalarına ihtiyaç vardır. Ayrıca, jeolojik-jeoteknik parametreler, inşaat maliyetleri ve mevcut altyapının mekansal dağılımı da bu amaçla dikkate alınmalıdır. Güncel arazi kullanımı/arazi örtüsü haritası ve buna bağlı olarak doğal tehlike duyarlılık haritaları yüksek çözünürlüklü uydu sensörlerinden elde edilebilmektedir. Bu çalışmada, heyelan ve sel doğal tehlikeleri göz önünde bulundurularak, gelişmekte olan bir kentsel yerleşim alanı için (Ankara, Mamak İlçesi, Türkiye) afet yönetimi amaçlı entegre bir doğal tehlike duyarlılık değerlendirmesi yapılmıştır. Ankara'ya ait taşkın duyarlılık haritası önceki bir çalışmada Değiştirilmiş Analitik Hiyerarşik Süreci (M-AHP) yöntemi kullanılarak üretilmiştir. Heyelan duyarlılık haritası ise Lojistik Regresyon tekniği kullanılarak bu çalışmada oluşturulmuştur. Bu amaçla güncel arazi kullanım haritası, Sentinel-2 görüntülerinin Rastgele Orman yöntemi kullanılarak sınıflandırılması ile oluşturulmuştur. Heyelan duyarlılık haritasının üretimi

için ayrıca yüksek çözünürlüklü dijital arazi modelinden elde edilen topografik parametreler ve Maden Tetkik Arama Kurumunun ürettiği litolojik bilgisi kullanılmıştır. Çoklu doğal tehlike duyarlılığı değerlendirmesi için Mamdani Fuzzy algoritması kullanılmış ve sonuçlar tartışılmıştır. Sonuçlar, kentsel planlama için altlık oluşturacak çoklu doğal tehlike duyarlılık haritalarının bir dizi makine öğrenmesi ve uzman tabanlı yöntemlerin birleştirilmesi ile elde edilebildiğini göstermektedir.

Anahtar Kelimeler: Çoklu Tehlike, Doğal Tehlike Duyarlılık Haritası, Heyelan, Taşkın, Kentsel Yerleşimler, Rastgele Orman, Lojistik Regresyon, Mamdani Fuzzy Algoritması.



ACKNOWLEDGMENTS

First, I would like to thank Assoc. Prof. Dr. Sultan Kocaman for supervising my thesis, supporting and leading my desire to work on disaster management. This thesis was completed more easily thanks to the attention she gave me in a new discipline I was involved in.

I also would like to thank Prof. Dr. Candan Gökçeođlu for expert opinions and giving valuable feedbacks about my work.

I deeply thank to the General Directorate of Mapping and the General Directorate of Mineral Research and Explorations for providing the data; and Recep Can, Burhan Sözer, Dr. Orhan Firat and Dr. Hakan A. Nefeslioglu from Hacettepe University for their endless help.

Lastly, I indebted to my extended family and friends for their continuous trust and faith.

Part of this thesis have been presented and published previously in ISPRS GeoInformation for Disaster Management 2019 Conference held in Prague, Czech Republic [Yanar, T.; Kocaman, S.; Gokceoglu, C. On the Use of Sentinel-2 Images and High Resolution DTM for Landslide Susceptibility Mapping in a Developing Urban Settlement (Mamak, Ankara, Turkey). In International Archives of the Photogrammetry, Remote Sensing & Spatial Information Sciences, Proceedings of the Geoinformation for Disaster Management (Gi4DM), Prague, Czech Republic, 3–6 September 2019; Vol. XLII-3/W8, pp. 469–476]; and ISPRS International Journal of Geo-Information [Yanar, T.; Kocaman, S.; Gokceoglu, C. Use of Mamdani Fuzzy Algorithm for Multi-Hazard Susceptibility Assessment in a Developing Urban Settlement (Mamak, Ankara, Turkey). ISPRS Int. J. Geo-Inf. 2020, 9, 114].

Tuğçe YANAR

April 2020, Ankara

TABLE OF CONTENTS

ABSTRACT.....	i
ÖZET.....	iii
ACKNOWLEDGMENTS.....	v
TABLE OF CONTENTS.....	vi
LIST OF FIGURES.....	viii
LIST OF TABLES.....	ix
ABBREVIATIONS.....	x
1. INTRODUCTION.....	1
2. BACKGROUND.....	4
2.1. Landslide Susceptibility Mapping.....	4
2.2. Flood Susceptibility Mapping.....	6
2.3. Multi-hazard Susceptibility Assessment.....	7
3. STUDY AREA AND INPUT DATASETS.....	12
3.1. The Study Area.....	12
3.2. Input Datasets.....	15
3.2.1. Digital Terrain Model.....	16
3.2.2. Sentinel-2 Imagery.....	16
3.2.3. Lithology.....	16
3.2.4. Flood Susceptibility Map.....	18
4. METHODOLOGY.....	21
4.1. Study Workflow.....	21
4.2. Preprocessing of Input Datasets.....	22
4.2.1. Topographic Derivatives.....	22
4.3. Image Classification with Random Forest Method.....	29
4.4. LS Map Generation with LR Method.....	30
4.5. MHS Assessment.....	31

5. RESULTS	34
5.1. Image Classification Results	34
5.2. The Landslide Susceptibility Results	35
5.3. Multi-Hazard Susceptibility Results	37
5.4. Elements at Risk	39
6. DISCUSSIONS	42
6.1. Mamak Urban Transformation Plan	42
6.2. 3D Models of Results.....	44
6.3. Urban Risk Management.....	47
7. CONCLUSIONS AND FUTURE WORK	49
7.1. Conclusions	49
7.2. Future Works	51
6. REFERENCES	53
APPENDIX.....	68
APPENDIX 1 - Publications derived from the thesis.....	68
APPENDIX 2 - Proceedings derived from thesis	69
APPENDIX 3 - Thesis Originality Report.....	70
CURRICULUM VITAE.....	71

LIST OF FIGURES

Figure 3.1. Master Plan of Ankara, 2023 [73].	13
Figure 3.2. Flood event in Boğaziçi Neighborhood on May 5, 2018 [75].	13
Figure 3.3. Landslide event occurred in Cengizhan Neighborhood on Nov 1, 2014 [76].	14
Figure 3.4. The research site and a general view of the Sentinel-2 image (top left coordinates : 32°56'51.372" E, 39°56'27.108" N; bottom right coordinates: 33°0'57.578" E, 39°53'41.689" N).	14
Figure 3.5. Sentinel-2 Coverage Map [81].	16
Figure 3.6. Lithology classes in the research boundary [79]	17
Figure 3.7. FS map of Ankara [19] and the test site of this thesis (the quadrangular section at the eastern part).....	19
Figure 3.8. FS map (revised version of Reference [19]).	20
Figure 3.9. Histograms of FS for five categories (very low, low, moderate, high, very high) on the left and three categories (low, moderate, high) on the right.....	20
Figure 4.1. The general workflow of the thesis.	22
Figure 4.2. The elevations and the landslide inventory (red polygons).	25
Figure 4.3. The slope and aspect maps.....	26
Figure 4.4. General curvature map.....	27
Figure 4.5. Plan and profile curvatures maps.	27
Figure 4.6. SPI map and TWI maps.	28
Figure 4.7. Proximity to channels and ridgelines.....	29
Figure 4.8. The membership functions of LS (on the left) and FS (on the right). The x- and y-axes show the susceptibility level interval and the degree of membership, respectively.	32
Figure 4.9. Overall framework of the Mamdani FIS constructed.....	33
Figure 5.1. LULC map as a result of the image classification.....	34
Figure 5.2. LS map obtained in this thesis.....	36
Figure 5.3. ROC curves of the LS map.	37
Figure 5.4. Multi-hazard susceptibility level map produced in this thesis.	38
Figure 5.5. Multi-hazard susceptibility level map produced in this thesis overlaid with the LULC.....	39

Figure 5.6. Buildings at the high MHSL areas.	41
Figure 6.1. Boundaries of implementation stages of Mamak Urban Transformation Plan [126].....	42
Figure 6.2. Mamak Urban Transformation Plan [126].....	43
Figure 6.3. A completed stage of Mamak Urban Transformation Project [127].	44
Figure 6.4. The digital terrain model that has a textured surface with the Sentinel-2 image.	45
Figure 6.5. The DTM that has a textured surface with LS map (result of LR method).	45
Figure 6.6. The digital terrain model that has a textured surface with the FS map.	45
Figure 6.7. The digital terrain model that has a textured surface with the MHSL map. The rings indicate significant focal spaces for urban planning in North-West and South Mamak as discussed before.....	46



LIST OF TABLES

Table 2.1. Use of different data sources for landslide susceptibility map production in the literature	5
Table 2.2. Use of different methods for landslide susceptibility map production in the literature	5
Table 2.3. Use of different methods for flood susceptibility map production in the literature	7
Table 2.4. Use of different methods for flood susceptibility map production in the literature.	10
Table 3.1. Characteristics of inputs.	15
Table 3.2. Common specifications of lithologies [79]	17
Table 4.1. Statistics of topographic derivatives	23
Table 4.2. Statistics of topographic derivatives in the landslide inventory	23
Table 4.3. Rule evaluation stage (if-then fuzzy rules) of the MHSL assessment.	32
Table 5.1. Classification accuracy of the image classification with Random Forest method	35
Table 5.2. Regression coefficients of the landslide conditioning parameters.	37
Table 5.3. Distribution rates of the MHSL.	38
Table 5.4. Distribution rates of the land use classes at high MHSL areas.	40

ABBREVIATIONS

Abbreviations

DEM	Digital Elevation Model
DSM	Digital Surface Model
DTM	Digital Terrain Model
FS	Flood Susceptibility
GLCM	Grey Level Co-occurrence Matrix
GSD	Ground Sampling Distance
LULC	Land Use Land Cover
LR	Logistic Regression
LS	Landslide Susceptibility
M-AHP	Modified Analytic Hierarchy Process
MHS	Multi-Hazard Susceptibility
MHSL	Multi-Hazard Susceptibility Level
MFA	Mamdani Fuzzy Algorithm
RGB	Red-Green-Blue
RF	Random Forest
SPI	Stream Power Index
TWI	Topographic Wetness Index

1. INTRODUCTION

Locally and globally enhanced hazard control is an essential focal point to decrease the damages resulting from natural hazards [1]. In developing countries, insufficient urban planning increases the adverse impacts of disasters on society economically and socially. The existing infrastructure and land use in urban planning are generally underestimated, yet they should be considered [2]. City planning is a complicated system that requires respect for existing conditions. This system can be supported by the current improvements in geographic information technologies like photogrammetry, 3D-GIS (Geographic Information System), remote sensing, volunteer contributions to geographical data, and high-level geographical analysis techniques for data acquisition and interpretation. In addition, these technologies provide crucial mechanisms to produce an integrated procedure.

Amongst the natural disasters related to climate and geology such as landslides, floods, quakes, wildfires, hurricanes, eruptions, cities are largely affected by landslides and floods. Constructions, substructure, and other amenities in the city can be damaged with a landslide that is one of the most prevalent natural risks with a worldwide expanse [4]. 23,041 number of landslides were seen in Turkey between 1950 and 2018 [5]. In the literature (e.g., References [6–10]), vast amount of research has been done on landslide susceptibility (LS), yet most research was on open lands and forests. Intensive structures that alter and mostly cover the topography makes LS assessment complicated in urban areas. Besides, more extended research is needed because of the complexness problem addition to unfinished and incorrect landslide inventories [11]. It is difficult to obtain LS maps at regional level because of the necessity of up to date data. These kinds of maps have importance for governments' disaster reduction actions.

Despite the diversity of landslide conditioning parameters, data availability is the principal restriction for used factors' numbers to generate LS. Generally, parameters like geomorphologic (e.g., topographic, hydrologic, etc.) and geologic (e.g. lithology) characteristics and land use and land cover (LULC) information must be taken into consideration for this purpose [4]. Representation of the geomorphological appearances in an urban area can be possible with a dense digital terrain model (DTM). Geological and geomorphological characteristics of the urban area change slowly unlike LULC. LULC currency is mandatory for obtaining high accuracy in the demonstration, due to

their importance for LS assessment [12]. Inventories are also used in the LS assessment models. Additionally, it is difficult to decide on landslide boundaries in residential lots and heavy construction zones in consequence of veiled or transformed topography, which significantly blocks the visibility of landslides.

Floods are additionally a notable natural hazard with its destructive effects, rate of fatality and occurrence frequency in the world [13,14]. The rate of flooding in Turkey is increasing day by day according to the statistics [15]. It is also expected that the rate of these events will continue to increase in the future with the result of climate change and rapid urbanization. Decision makers should examine flood susceptibility (FS) maps since they contain valuable information that can be used in urban mitigation plans [16-18]. Sozer et al. [19, 20] generated FS map using a modified analytical hierarchy process (M-AHP) [21] that is an expert-based decision support system was used to produce for Ankara, Turkey. As it will cause inadequate and inaccurate results to be created in a small area similar to the study area, using the outputs obtained from this study, where FS is evaluated at the regional level will increase the accuracy rate of the study. The east part of this flood susceptibility map was cropped, reclassified and added to the multi-hazard susceptibility (MHS) evaluation process in this research.

Moreover, landslides and floods are generally remarkable in the areas that have similar geographical and ecological situations. Flood events might trigger landslides when the amount of rainfall is high. For this reason, these two types of natural hazards need to be evaluated together. The assessment allows detailed analysis of the effects of landslides and floods both separately and together.

The principal purpose of this thesis was to formulate a methodology for creating MHS maps that can form the base of city planning stages. The Mamak region, a central district in Ankara, Turkey, which is subject to development projects, was found suitable for this purpose of the study. For this reason, the eastern part of the Mamak region was selected as study area. With this study, the Urban Transformation Project being carried out Mamak region is examined from the issue of sensitivity to natural hazards. At the same time, the infrastructures that the region should have within the framework of risk management could be evaluated accordingly.

In the thesis, first, the actual land use map was created using Sentinel-2 satellite images and topographic parameters were created using the high-resolution digital

elevation model (DEM), and lithology data was obtained from the existing geospatial database [4]. These parameters were employed in the production of the LS map. As mentioned before, FS maps are required to be created at regional scale. For this reason, the FS map of Ankara generated by Sozer et al [19,20] was utilized in this thesis after cropping and reclassification. Then, the Mamdani fuzzy algorithm (MFA) was used to create the MHS map. Outputs were visualized and examined in 2D and 3D formats. Existing settlements' conditions and multiple hazard risks were evaluated together within the scope of city planning. This is one of the first studies in the literature in which the MFA is used to evaluate two hazard susceptibility maps together.

A literature background for landslide, flood, and multi-hazard susceptibility is presented under the next, the second main Chapter, in this thesis. In the third Chapter, the study area and features of the input data are explained. The methodologies used in the study are expounded in detail in the fourth Chapter. Results are examined under the fifth Chapter. Under the sixth Chapter, the final products are discussed with an urban transformation plan and three-dimensional images. In the last Chapter, a general conclusion of the work and how it can be improved with future studies are mentioned.

2. BACKGROUND

2.1. Landslide Susceptibility Mapping

Incidences of natural disasters are gradually increasing worldwide. For this reason, the detection of natural hazards with automated systems becomes important. Landslides are the events that frequently turn into disasters throughout the world. Therefore, most of the studies have focused on this subject in the literature. Different sources such as SAR, Lidar and stereo images are used for the detection of landslides in the literature [22-25]. Also, many different methods are used in the production of maps. Some of these are support vector machine (SVM) [26-28], artificial neural network [28-31], fuzzy logic [28,32], analytical hierarchy process [32-34], statistical index and weighting factor [33-34], and logistic regression (LR) [29-30,34] methods. Similar landslide conditioning parameters were also used in most of the studies mentioned above (e.g. slope, curvature, soil drainage, soil texture, topographic wetness index, channel order, soil map, land cover and lithology)

Although two-class SVM is more accurate than the LR method in the study of Yao et al. [26], the results are less sensitive than all of them in one-class SVM. Moreover, as mentioned in the study, the use of the SVM method is notably suitable in studies about landslide susceptibility assessment with a small number of training sample. However, according to the comparison made in Pradhan's study [28], ANFIS method yielded higher accuracy than SVM method.

In another study, the fuzzy logic method and AHP method were compared and it was seen in the Receiver Operating Characteristic (ROC) curve that more accurate results were obtained in the fuzzy logic method [32]. It was stated that AHP method, which is based on expert opinion, was directly affected by the subjectivity and this situation may be the reason for the decrease in the level of accuracy. In the study where the AHP method is compared with other methods (statistical index and weighting factor) [33] and the last mentioned study, the accuracy level in the AHP method is almost the same. This may indicate that the AHP method generally gives a similar range of accurate results. The success of the artificial neural network method in producing LS map has also been mentioned in many studies [e.g. 28-30].

As seen in many studies and will be explained in more detail later in the thesis, the LR method is a popular method for producing LS maps, which provides fast and

accurate results. Therefore, in this thesis, it has been decided to use the LR method for producing the LS map.

According to Fell et al. [35], the study goals, parameters, methods, landslide inventory, field properties, etc. affect the results of the study. In short, the precision of the methods should not be evaluated independently of the data. A general overview of the literature on landslide susceptibility mapping methods is given in Table 2.1. and Table 2.2.

Table 2.1. Use of different data sources for landslide susceptibility map production in the literature

Authors	Data Sources for Landslide Susceptibility Map Production
Jaboyedoff, M. et al. [22]	Lidar
Colesanti, C. and Wasowski, J. [23]	SAR
Chen, W. et al. [24]	Lidar
Weirich, F. and Blesius, L. [25]	Satellite and Air Photo

Table 2.2. Use of different methods for landslide susceptibility map production in the literature

Authors	Methods for Landslide Susceptibility Map Production	Authors	Methods for Landslide Susceptibility Map Production
Nefeslioglu, H. A. et al. [6]	Artificial Neural Network	Sevgen, E. et al. [10]	Logistic regression, Artificial Neural Network and Random Forest
Yao, X. et al. [26], Brenning, A. [27]	Support Vector Machine	Pradhan, B. [28]	Decision Tree, Support Vector Machine and Neuro-Fuzzy Models

Yesilnacar, E. and Topal, T. [29]	Logistic Regression and Neural Networks	Pradhan, B. and Lee, S. [30]	Artificial Neural Networks, Frequency Ratio and Logistic Regression
Lee, S. et al. [31]	Artificial Neural Network	Pourghasemi, H. R. et al. [32]	Fuzzy Logic and AHP
Yalcin, A. [33]	AHP and Bivariate Statistics	Yalcin, A. et al. [34]	Frequency Ratio, AHP, Bivariate Statistics and Logistics Regression

2.2. Flood Susceptibility Mapping

Producing flood susceptibility maps is also important for disaster management like landslides. Many methods are used in the literature for the production of FS maps. Similar to LS map production, AHP [19-21], SVM [36-37], decision tree [37-38], LR [39-40], random forest [40-41], entropy, statistical index, and weighting factor [42] and neuro-fuzzy inference systems (ANFIS) [43] methods are used for this purpose. Besides, when the methods were used as hybrids, it was mentioned that the precision of the results is adequate [36]. Although the parameters used in the above studies are similar to those used in the creation of LS maps (e.g. slope, topographic wetness index (TWI), stream power index (SPI), and lithology), parameters like sediment transport index, flood accumulation, normalized difference vegetation index (NDVI), rainfall, distance to the river are also included.

As discussed in the study of Tehrany et al. [37], the contribution of each parameter to the accuracy of the method is different. In the study, it was observed that not every data added to the dataset increased the precision, and some elements (e.g. geology and slope) were highly correlated. Also, different methods were found to achieve the highest accuracy results on different datasets.

It is possible to reach accurate and precise results with study areas including basin in FS maps. In the study of Sozer et al. [21], FS map was generated with the M-AHP method with similar parameters (i.e. flow accumulation, slope gradient, elevation, distances to permanent river and dry drainage, land cover, TWI, and lithology). This map also covers the study area of this thesis. For this reason, this map was used in this thesis

to reach accurate results. A general overview of the literature on flood susceptibility mapping methods is given in Table 2.3.

Table 2.3. Use of different methods for flood susceptibility map production in the literature

Authors	Methods for Flood Susceptibility Map Production	Authors	Methods for Flood Susceptibility Map Production
Sozer et al. [19-21]	M-AHP	Hong, H. et al. [36]	Logistic Regression, Random Forest and Support Vector Machines
Tehrany, M. et al. [37]	Support Vector Machine, Decision Tree	Khosravi, K. [38]	Decision Tree
Tien Bui, D. et al. [39]	Logistic Regression	Chapi, K. et al. [40]	Logistic Regression, Random Forest
Lee, S. et al. [41]	Random Forest	Khosravi, K. et al. [42]	Entropy, Statistical Index, and Weighting Factor
Razavi Termeh, S. V. et al. [43]	Neuro-Fuzzy Inference Systems (ANFIS)		

2.3. Multi-hazard Susceptibility Assessment

Cities are affected by various disasters. Risk estimation should be made precisely to control the possible impacts of future disasters. It is also important to evaluate more than one disaster risk that has the potential to occur in a region. For this purpose, MHS assessment models can be created with different methods. Furthermore, more efficient results are obtained by using multilayered information in disaster management [44]. Susceptibility maps can be created with several methods by using different parameters.

Using one of these methods, AHP, the weight ratios of each disaster are decided by the professionals [45-47]. Achieving hazard, exposure, vulnerability, and risk outcomes is another method as a result of the gradual analysis of all parameters that cause natural risks [48]. Mukhopadhyay et al. [49], on the other hand, used the multi-criteria decision analysis (MCDA) method in generating the multi-hazard susceptibility map, although similar inputs were used (multiple and non-homogeneous). The sensitivity of the parameters weighted by experts is considered important and it was declared that this situation increased the precision of the outcomes in all studies. In Chen et al. [50], each type of hazard was analyzed in four scenarios. Injuries caused by the per disaster were calculated separately. Then three features were multiplied by the multiplication method (quantity and the spatial likelihood of components at danger and physical resistance). The impact of each type of disaster was found comparable to these outcomes.

According to Ehlen and Vargas [51], while evaluating disaster risks collectively, one should also consider social and economic aspects. As an integrated risk assessment of China, four classes of determinants, i.e. population exposed to many hazards, economic susceptibility, the coping power of management and social infrastructure and adaptation power to future natural disasters was used to create China's disaster risk index [52]. Additionally, risk exposure and risk injury were examined as an exposure parameter. In the study of Tian et al. [53], the extent of the parameters was enlarged. The resilience of the society to disaster risks was measured by using multiple linear regression method. Also, the researchers suggested that this method can be improved with expert data and entropy. In other studies, it has been stated that these parameters may be insufficient for multi-hazard assessment and the regions where natural disasters occur should be examined by adding human actions [54-55]. In addition, it is thought that the climate characteristics of the area should be included in the assessment of multiple natural disasters [44,55].

It has been proposed to use an algorithm based on overlapping each risk value and possible interactivity between hazards when operating with restricted data [56]. Potential multi-hazard risks were calculated for each combination by using matrix that shows risk combinations and potential interactions between risks with this algorithm. The use of the MmhRisk - HI (Model for multi-hazard Risk assessment with a consideration of Hazard Interaction) mechanism, which consists of two principal elements, is another multi-hazard susceptibility assessment method [57]. The primary element is the analysis of the

relations in disaster, other disasters and their surroundings. The level of relationship between disasters (independent, parallel etc.) is used in multiple hazard existence probability with using special functions in this element. The secondary element is probable injuries and destruction rate computed using the Bayesian network method. The use of a completely probabilistic multi-hazard risk (MHR) model is another approach [58]. In this approach, annual mean and max loss rates were computed using stochastic case collections. According to Micu et al. [59], quantitative MHR assessment with regions at risk, exposures, and vulnerabilities) became prominent to make regional multi-hazard risk assessments. As another quantification strategy mentioned by Tilloy et al. [60], the relationship between natural disasters was examined in two contexts. These are called cascading hazards and compound hazards created by stochastic, empirical, mechanistic methods. Yet, according to the study, it is mentioned that mechanistic and stochastic techniques have some limitations (e.g. analytical uncertainties, data quality) within the framework of multi-hazard assessment.

Evaluating various disaster risks collectively and predicting possible hazards in cities can be beneficial for city planners to prioritize their decisions and control risks and possible losses in the more appropriate approach [54,61-63]. In some studies, although the consequences of the hazards in the cities were analyzed separately, a quantitative strategy was required in the collective evaluation of hazards (e.g. [61,64]). Comparing natural disasters collectively with a quantitative method rather than forming a visual comparison of disasters one by one gives more precise outcomes. In addition to the quality of the data, choosing the right parameters and weighting them correctly has great importance. However, according to Kappes et al. [65], another important point is choosing the right method (i.e. qualitative, semi-quantitative, or quantitative methods) according to the objectives. In this context, in another study, the results of MHR assessment were achieved by applying the theory of probability and Boolean logic methods on different combinations of hazard risks [66].

Besides all these methods, machine learning (ML) methods used in many fields are appropriate for multi-hazard risk evaluation. In the study of Liu et al. [67], the multi-hazard analysis was performed by combining hazard maps created with the random forest method. The results of the model have a considerably high accuracy rate, which supports the use of ML methods for this purpose. TOPSIS namely Technique for Order of Preference by Similarity to Ideal Solution was also applied as a multi-criteria decision-

making model [68]. In this study, similarity indexes were created for each disaster and multiple hazard maps were produced. In Reference [69], the TOPSIS technique was combined with Mahalanobis distance and simple additive weight (SAW) techniques. Although the use of the TOPSIS method in susceptibility map production causes criticism due to operating with just a geometric distance, it has also been observed that it produces more explicit outcomes than some methods.

Some researches using multi-criteria decision-making methods have also been conducted. Use of SWARA namely Stepwise Weight Assessment Ratio Analysis and ANFIS namely Neuro-Fuzzy Inference System technique, a fuzzy inference system namely FIS, is an example of this use [70]. The weighted overlay analysis method was used as another method for the analysis of hazard maps collectively [49]. Besides, the use of fuzzy models has made many operations possible. In the study of Araya-Munoz et al. [71], the correlations between parameters were examined applying the gamma fuzzy overlay model. There are many methods for combined assessment of natural disaster risks and each method has many difficulties [72]. The multi-hazard assessment, which has a great role in disaster management, was produced in this study using the Mamdani fuzzy inference algorithm. A general overview of the literature on multi-hazard susceptibility mapping methods is given in Table 2.4.

Table 2.4. Use of different methods for flood susceptibility map production in the literature.

Authors	Methods for Multi-Hazard Susceptibility Map Production	Authors	Methods for Multi-Hazard Susceptibility Map Production
Bathrellos, G. et al. [45], Skilodimou, H. et al. [46], Bani-Mustafa, T. [47]	AHP	Mukhopadhyay, A. et al. [49]	Multi-Criteria Decision Analysis (MCDA), Weighted Overlay
Chen, L. et al. [50]	Multiplication Method	Tian, C. et al. [53]	Multiple Linear Regression Model

Barrantes, G. [56]	Overlapping	Liu, B. et al. [57]	MmmhRisk - HI
Tilloy, A. et al. [60]	Mechanistic and Stochastic Methods	Omidvar, B. and Karimi, H. [66]	Boolean Logic Method
Liu, K. et al. [67]	Random Forest	Mirzaei, G. et al. [68]	TOPSIS
Sheikh, V. et al. [69]	TOPSIS+Mahalanobis Distance and SAW	Pourghasemi, H. R. et al. [70]	SWARA, ANFIS, FIS
Araya-Munoz, D. et al. [71]	Gamma Fuzzy Overlay Model		

3. STUDY AREA AND INPUT DATASETS

3.1. The Study Area

Urban sprawl is one of the main problems for urbanization nowadays. As a developing country, Turkey is suffering from urban sprawl. Mamak District is positioned in the east part of Ankara, Turkey and subjected to rapid urban transformation. As can be seen in the 2023 Master Plan of Ankara (Figure 3.1), Mamak area is the one part of the urban sprawl of Ankara like Etimesgut, Gölbaşı, Pursaklar, Sincan etc. [73] Almost 640 thousand people live in this region [74]. Mamak has an important part of the essential technical infrastructure in the city. Close proximity to the railway, highway and other transportation options makes this part of the city a development focus. In addition to the transportation infrastructure, east part of Mamak is used for the recreational purpose in Bayındır Dam. There were some landslides and flooding in some part of the Mamak District and it is known that other parts of the district are also prone to both landslides and flooding. For instance, the flood event occurred in Boğaziçi Neighborhood, Mamak as a result of precipitation on May 5, 2018. Many people injured and many property damages occurred (Figure 3.2) [75]. As mentioned by the Ankara Chamber of Civil Engineers, the Hatip Stream region, which is flooded is the region where the flood caused the most casualties of the history [75]. Also, the landslide event that took place in Cengizhan Neighborhood on November 1, 2014, is one of the cases of landslide in Mamak (Figure 3.3). Landslide formation was observed in the same neighborhood between 2011 and 2012 [76]. As mentioned by the Chamber of Geological Engineers, the area was not prepared for the landslide hazard considering the settlement characteristics, which could even trigger the landslide [77]. In addition, Mamak Urban Transformation Plan is involving these areas. Study area was selected by considering these conditions (Figure 3.4). The region covers 30 km². The min elevation is 924 m and max elevation is 1284 m.

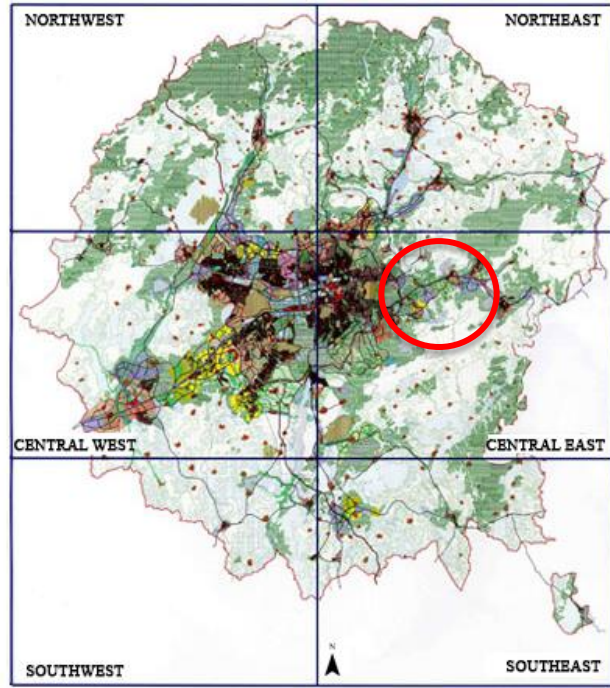


Figure 3.1. Master Plan of Ankara, 2023 [73].



Figure 3.2. Flood event in Boğaziçi Neighborhood on May 5, 2018 [75].



Figure 3.3. Landslide event occurred in Cengizhan Neighborhood on Nov 1, 2014 [76].

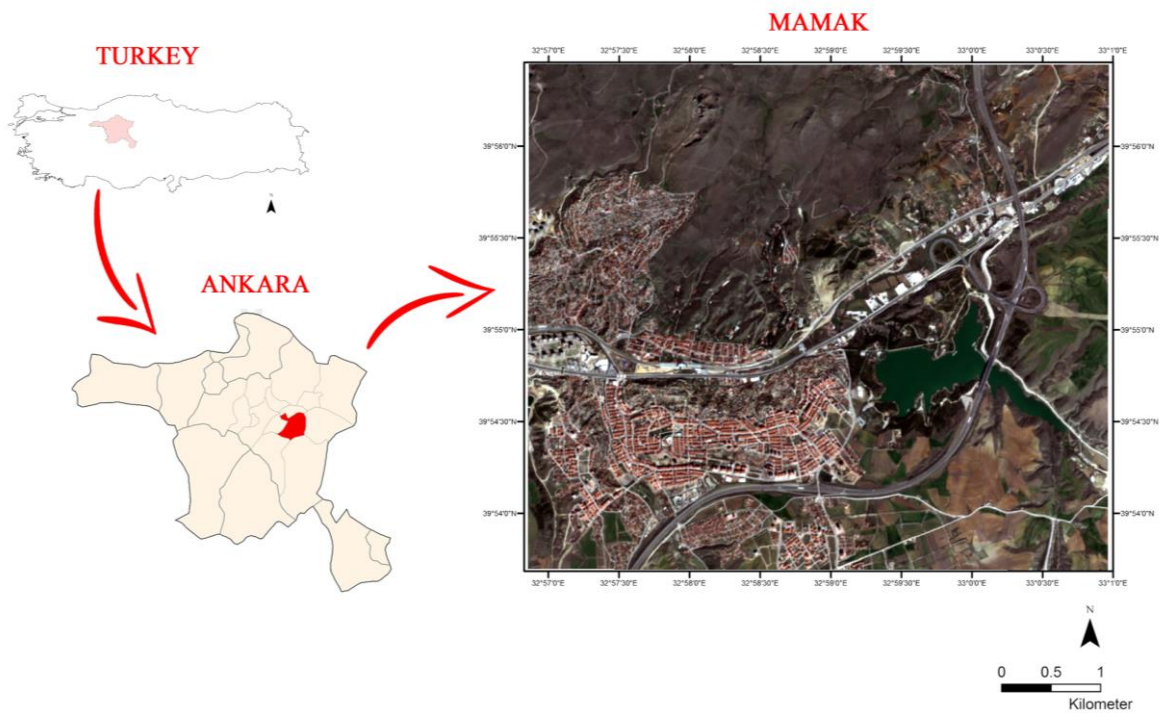


Figure 3.4. The research site and a general view of the Sentinel-2 image (top left coordinates : $32^{\circ}56'51.372''$ E, $39^{\circ}56'27.108''$ N; bottom right coordinates: $33^{\circ}0'57.578''$ E, $39^{\circ}53'41.689''$ N).

3.2. Input Datasets

General Directorate of Mapping (GDM), Turkey provided a DTM that has a 5-m resolution. Some topographical parameters and derivatives i.e. altitude, slope gradient, curvatures (general, plan and profile), TWI, SPI, distances to channels and ridgelines were acquired from the DEM. On March 23rd, 2019, Sentinel-2 imagery was acquired from the ESA Copernicus Open Access Hub [78]. This imagery is used for classification of LULC using the random forest (RF) method, one of the supervised classification methods. The WebGIS portal of the General Directorate of Mineral Research and Exploration (GDMRE/MTA), Turkey [79] provides lithology data freely. It was digitized into vector form and transformed into a raster form with 5-m resolution. LULC created from the Sentinel-2 imagery with a 10-m resolution has also been resampled to the 5-m resolution. The reason for this is to ensure that the input parameters of the susceptibility map to be created with the LR technique have the same features. The input resources and spatial resolutions are given in Table 3.1. The extents of actual landslides comprising approximately 2000 grid points were drawn manually by the specialist to compute the LR coefficients using a digital terrain model and the Sentinel-2 images.

Table 3.1. Characteristics of inputs.

FACTORS	DATA ORIGIN/METHOD	GSD*
Geomorphology	DEM	5m
LULC	Generated with Sentinel-2 image classification with RF	10m (upsampled to 5m)
Lithology	MTA Yerbilimleri Web Portal	5 m
LS Map	Generated with LR	5 m
FS Map	Received from prior studies of Sozer et al. [19,20]	5 m

* GSD: Ground Sampling Distance

3.2.1. Digital Terrain Model

Topographic features of a basin are an important resource for understanding the hydrological and geomorphological processes of the region [80]. The most important resource used to perform the analysis of the topography is the DEM, which is a digital terrain model (DTM) here. The DTM with 5-m resolution was constituted by GDM with the airborne photogrammetric flight and was used as topographic data source in this study.

3.2.2. Sentinel-2 Imagery

The Sentinel-2 is an multi-band ground observation satellite launched and operated by the European Space Agency [78]. The RGB bands has 10m GSD and high transition frequency [81]. Although the repetition of moving through the same orbit is 5 days, the number of viewing the same place again is superior in connection with overlapping orbits (Figure 3.5). These images were preferred because they are provided by ESA free of charge and have high spatial resolution and 13 spectral bands. It is also popularly used in natural hazard analyses [82].

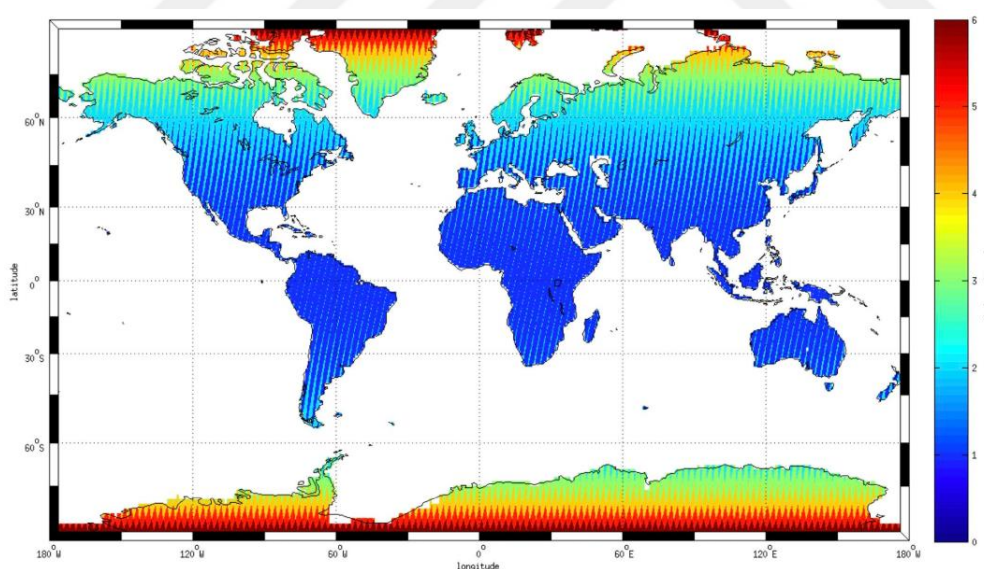


Figure 3.5. Sentinel-2 Coverage Map [81].

3.2.3. Lithology

The lithology classes are remarkably essential for natural hazard analysis like LULC and DTM [83]. The geological characteristics of the area can be examined with

the lithological descriptions. Durableness and transmissivity of rocks and soils can be affected with the lithological and structural differences in general [84]. The lithology data was provided by the Yerbilimleri portal of MTA. Five classes located in the study area are given in Figure 3.6, and their specifications are given in detail in Table 3.2. A raster dataset with 5-m resolution was generated by converting this vector map.

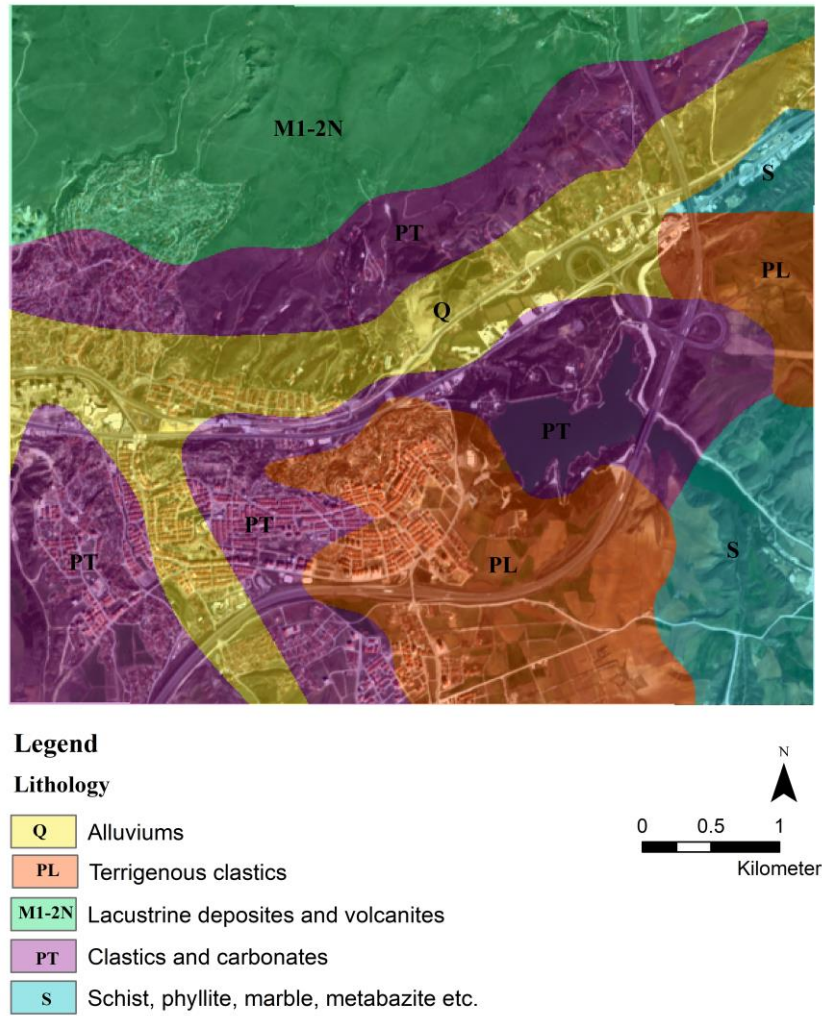


Figure 3.6. Lithology classes in the research boundary [79]

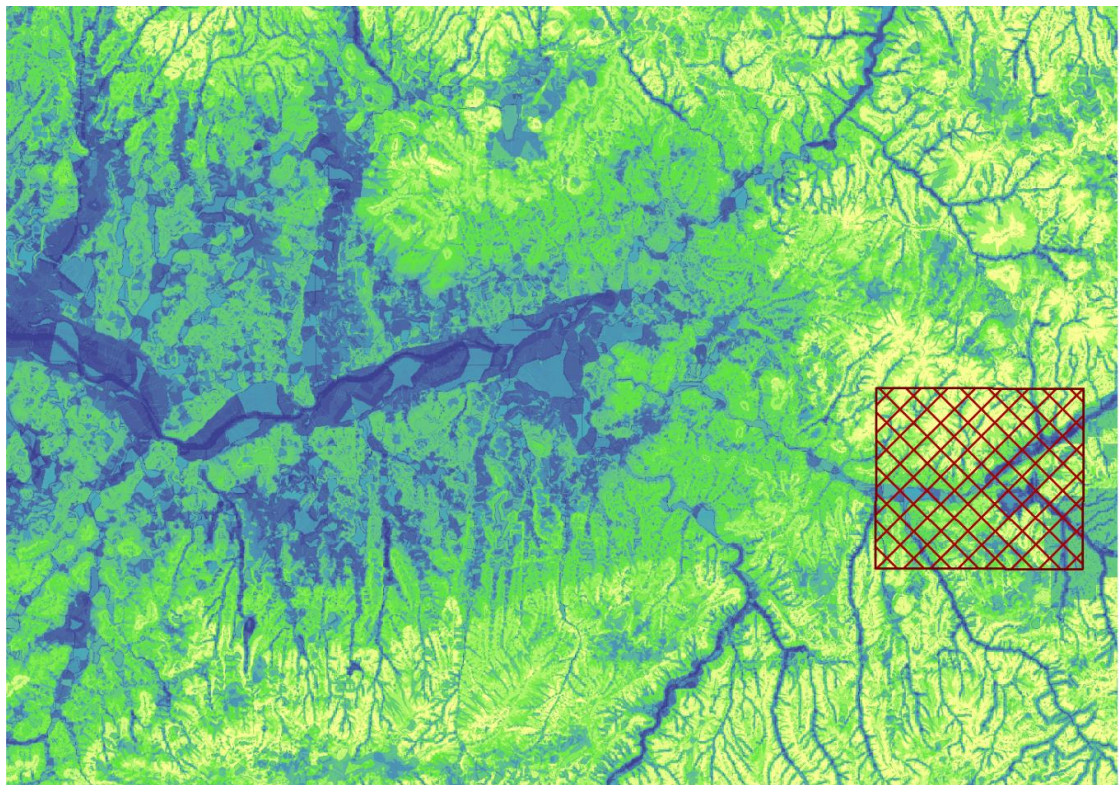
Table 3.2. Common specifications of lithologies [79]

AGE	DESCRIPTION
Quaternary	Alluviums
Pliocene	Terrigenous clastics

Early – Middle Miocene	Lacustrine deposits and volcanites
Permo - Triassic	Clastics and carbonates
Late Paleozoic-Triassic	Schist, phyllite, marble, metabasite etc.

3.2.4. Flood Susceptibility Map

Figure 3.7 shows the FS map belonging to the metropolitan region of Ankara. It was received from prior studies of Sozer et al. [19,20]. In this research, the M-AHP method [21] based on analytical hierarchy is used for generating FS map using diverse parameters like topographical parameters (flow accumulation, slope, topographic altitude, etc.), land cover, and lithology parameters. In the M-AHP method, each parameter has weights in reference to expert evaluation and the rates of the scores define priorities. Equal class intervals are used for classifying FS to five classes in Sozer et al. [19]. Since the LS map was composed in three classes in this thesis, the FS map was clipped and then reclassified into three classes with equal intervals. Figure 3.8 demonstrates the FS map of the study area. The FS map classes used for MHS assessment are defined as low, moderate and high. Statistics of the classification descriptions in Sozer et al. [19] and new classification are given in histograms (Figure 3.9).



Flood Susceptibility

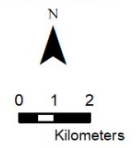
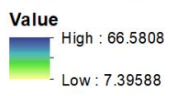


Figure 3.7. FS map of Ankara [19] and the test site of this thesis (the quadrangular section at the eastern part).

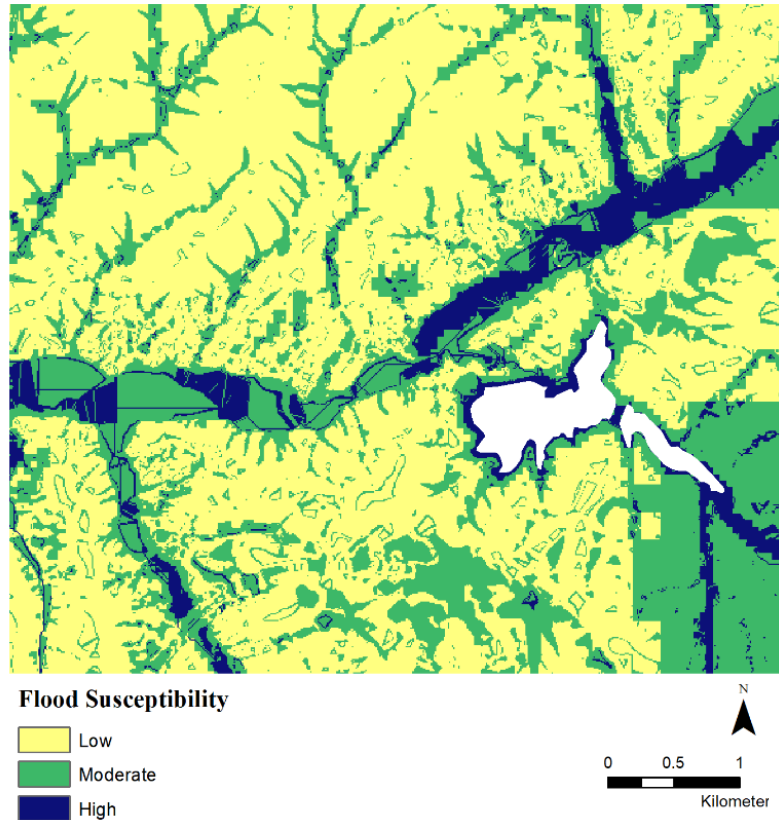


Figure 3.8. FS map (revised version of Reference [19]).

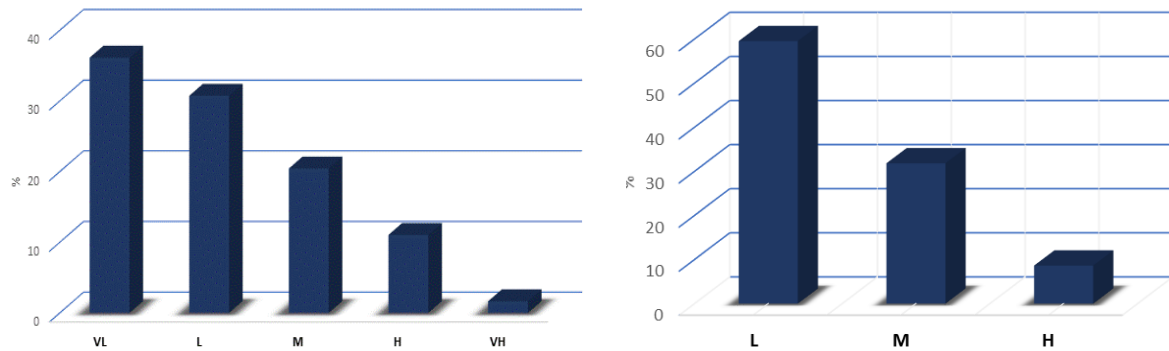


Figure 3.9. Histograms of FS for five categories (very low, low, moderate, high, very high) on the left and three categories (low, moderate, high) on the right.

4. METHODOLOGY

4.1. Study Workflow

The LR method is used for obtaining the LS map of the study zone by using LULC (generated from Sentinel-2 satellite imagery), topographic derivatives (generated from DEM), and lithological data [4]. ESA serves Sentinel-2 images freely with 13 spectral bands at 10-20-60m GSDs. They are improved (orthorectified, L2A) geometrically and gathered annually over a wide geographic coverage by ESA [78]. In addition, the satellite constellation has a great transmittal rate [81]. For these reasons, it is extensively utilized in natural hazard assessment [82]. So, Sentinel-2 images were found useful for the production of the up-to-date land-use data. Sentinel-2 images can be easily processed with the Sentinel Application Platform (SNAP) Tool supplied by ESA. This makes Sentinel-2 images suitable for urban planners with little remote sensing knowledge. The method used in producing the LS map required to be capable of processing non-numerical parameters like lithology types. In this case, the LR method is simpler and more convenient than other methods. In the LS maps created with this method, the probabilities are classified and examined as low, moderate and high. Landslide and flood susceptibility maps will be evaluated together under the MHS assessment model. The FS map was obtained from Sozer et al. [19]. Additively, the FS grouped under five levels from very low to very high were reclassified into three levels (i.e., low, moderate, and high) to be utilized as input in the MHS. The thesis workflow is described in Figure 4.1. Detailed information about inputs and methodologies is given in the lower parts of the headings.

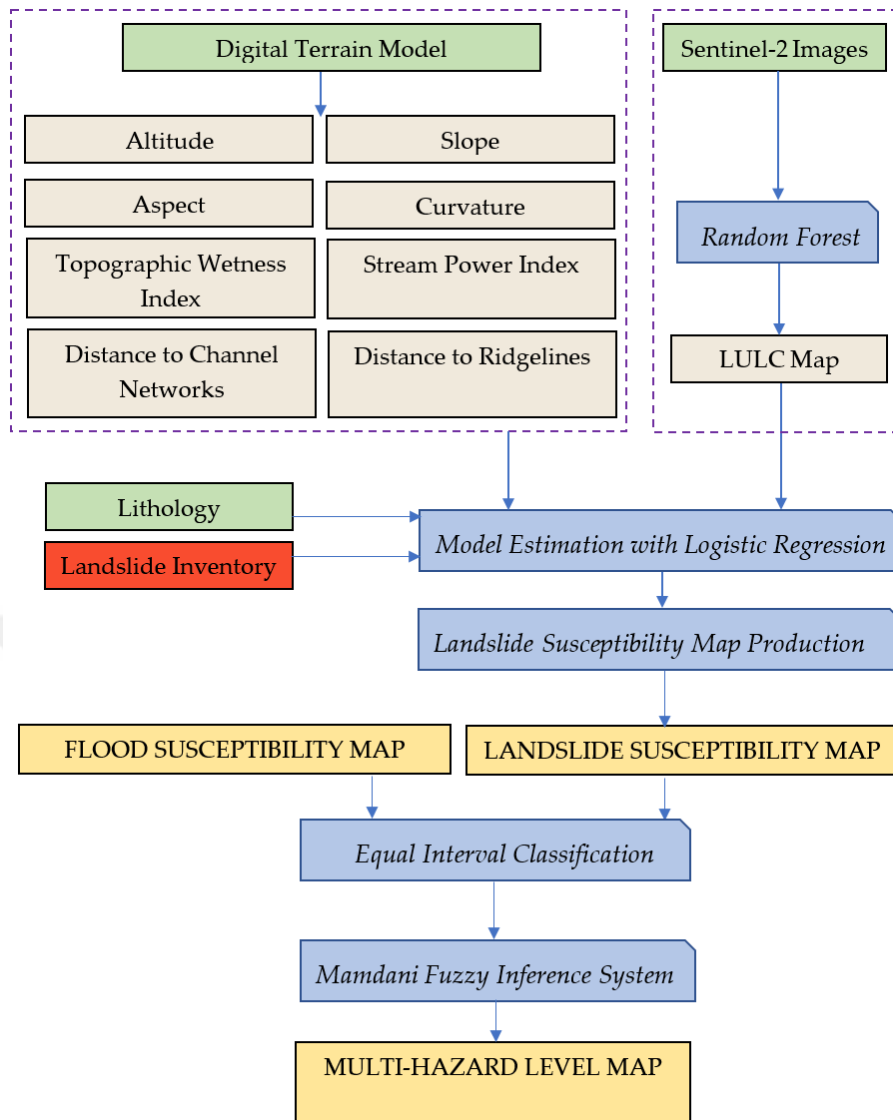


Figure 4.1. The general workflow of the thesis.

4.2. Preprocessing of Input Datasets

4.2.1. Topographic Derivatives

Regions are defined as some topographical attributes such as first and second derivatives of a digital terrain model for understanding the topography. Primary features like slope gradient, aspect, general curvature, etc. are determined by using altitude data while secondary features like stream power index and topographic wetness index are determined by using secondary derivatives of altitude data [80]. SAGA GIS [85] and ArcGIS [86] software were employed in this thesis for calculating topographic derivatives. Table 4.1 represents a statistical review of the altitude data and its derivatives.

Similar results were acquired for the actual landslide samples (approximately 2000 grid points) and are represented in Table 4.2.

Table 4.1. Statistics of topographic derivatives

ATTRIBUTE NAME	MIN	MAX	MEAN	STD. DEV.
Elevation (m)	924.1	1284.7	1032.2	62.8
Slope (degree)	0.004	73.127	13.075	8.719
Aspect (degree)	0	360	192.23	101.46
General Curvature	-1.25957	1.09325	-9.73E-05	0.05887
Plan Curvature	-0.09291	0.14917	4.56E-04	9.69E-03
Profile Curvature	-0.16431	0.16666	-5.05E-04	0.01107
SPI	0	3315271.5	688.02	14974.51
TWI	1.2776	22.1526	5.8651	2.1451
Distance to Channel (m)	0.4	561.9	84.2	73.8
Distance to Ridgeline (m)	0.0	229.9	33.0	26.5

Table 4.2. Statistics of topographic derivatives in the landslide inventory

ATTRIBUTE NAME	MIN	MAX	MEAN	STD. DEV.
Elevation (m)	934.4	1050.4	986.5	30.7
Slope (degree)	0.560	39.793	20.171	7.949
Aspect (degree)	0.64	359.59	233.03	80.38
General Curvature	-0.369	0.388	-0.0094	0.0943
Plan Curvature	-0.0717	0.0493	-0.00418	0.0187

Profile Curvature	-0.05139	0.04435	-0.00454	0.0139
SPI	0.362	9091.607	319.292	814.8529
TWI	2.2736	15.33	5.197	1.719
Distance to Channel (m)	0.4	142.3	44.1	40.7
Distance to Ridgeline (m)	0.0	50.4	15.7	10.9

4.2.1.1. Landslide Inventory

The landslide inventory prepared as vector polygons was rasterized in with 5-m grid spacing to use in the LR model estimation process. The landslides identified in the field transpired in schists and volcanic units, which are very responsive to weathering and landslides. The principal features of the landslides were orbicular, and the deepness of collapsed covers was examined by the density of weathered regions. Besides, the destruction of the constructions in the study field was discerned, and it is known that the main reason for the destruction is the landslides. Yet, it is difficult to specify the boundaries of the landslides because of the urbanization on the downslopes. Landslide inventory drawn by the red polygons are given in Figure 11.

4.2.1.2. Altitude

Altitude demonstrates range and measurements of the elevation in the site [87]. The altitude indicates the roughness of a surface and affects the abrasive processes, accordingly it is used in the production of landslide susceptibility maps [88]. The altitudes are given in Figure 4.2.

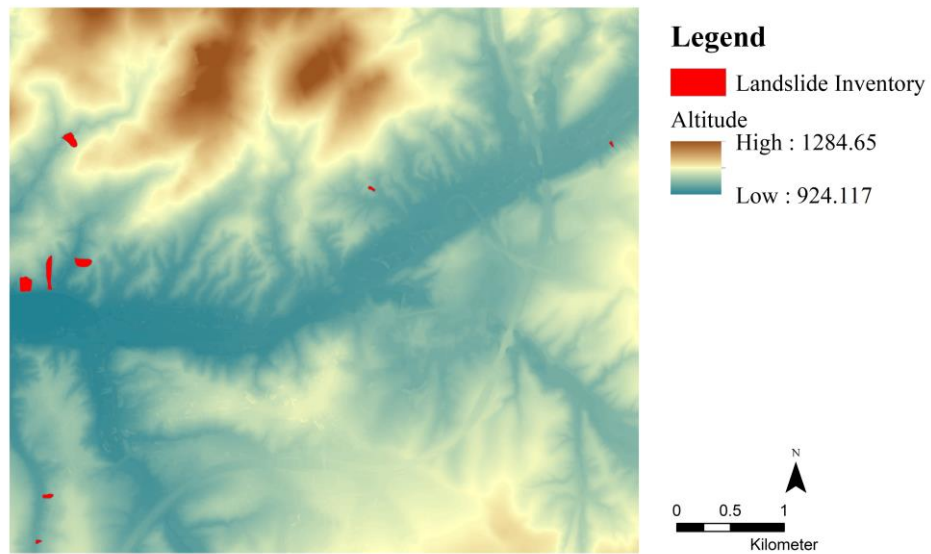


Figure 4.2. The elevations and the landslide inventory (red polygons).

4.2.1.3. Slope and Aspect

A measure of the variety in height rate is expressed as a slope gradient [87] (Figure 12). In this study, slope gradients are used for making a connection between changes in the topography and landslide formation. Landslide risk increases in regions with high slopes (exceed 20°) [89].

The aspect is calculated as the path of the most perpendicular descending line. It is computed clockwise originating from North. Aspect values define 360° in the East, 270° in the South, 180° in the West, and 90° in North. Slope directions (north, south, etc.) can be linked with the affection rate of the landslides [87]. Aspect is associated with parameters that can control the formation of landslides such as precipitation, wind effect and exposure to sunlight [89]. Figure 4.3 shows the aspect map of the test site.

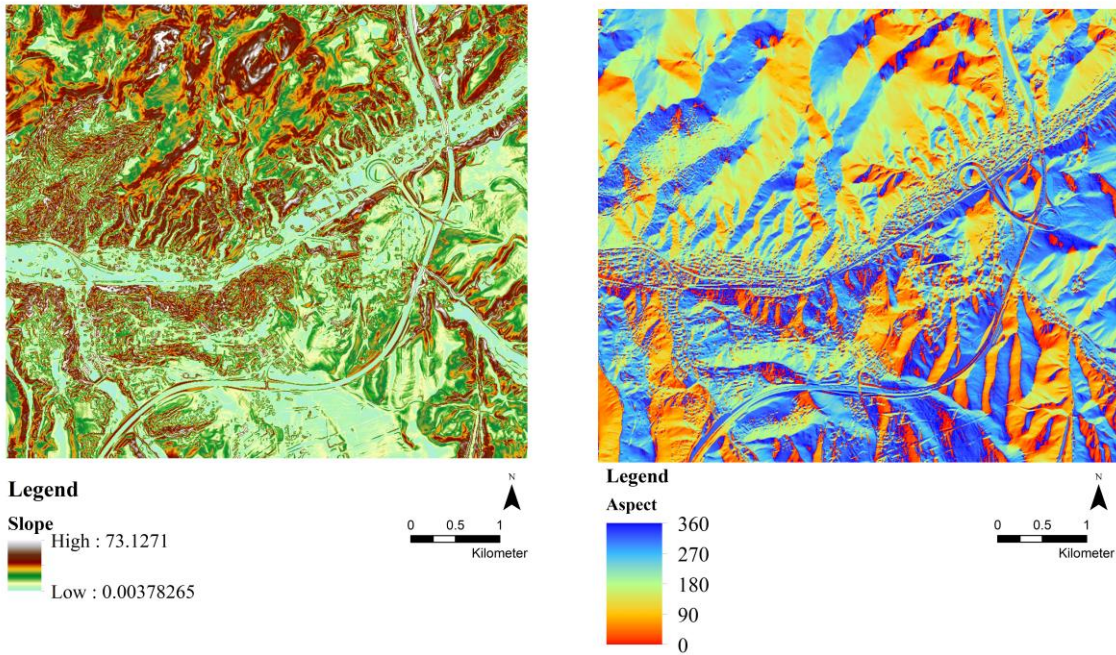


Figure 4.3. The slope and aspect maps.

4.2.1.4. Topographic Curvatures

The general curvature reflects the overall change in slope and aspect and shown in the Figure 4.4. Also, general curvatures can be examined separately as a planimetric and profile curvatures. The slope change along the contour lines generates the planimetric component and the rate of change in the slope gradient shapes generates profile component [87]. Figure 4.5 shows the plan and profile curvatures in the site. Surface concavity indicates that curvatures are negative, and the surface convexity indicates that curvatures are positive and surface flatness indicates that curvatures are zero [90]. The curvature rates describe the morphology of the topography. The effect of the curvature (concave, convex, flat) ratios of the surface and the accumulation of water on the surface, by considering the changes in slope and aspect, was provided with this parameter [91]. Also, most landslides are observed in flat and concave regions [88].

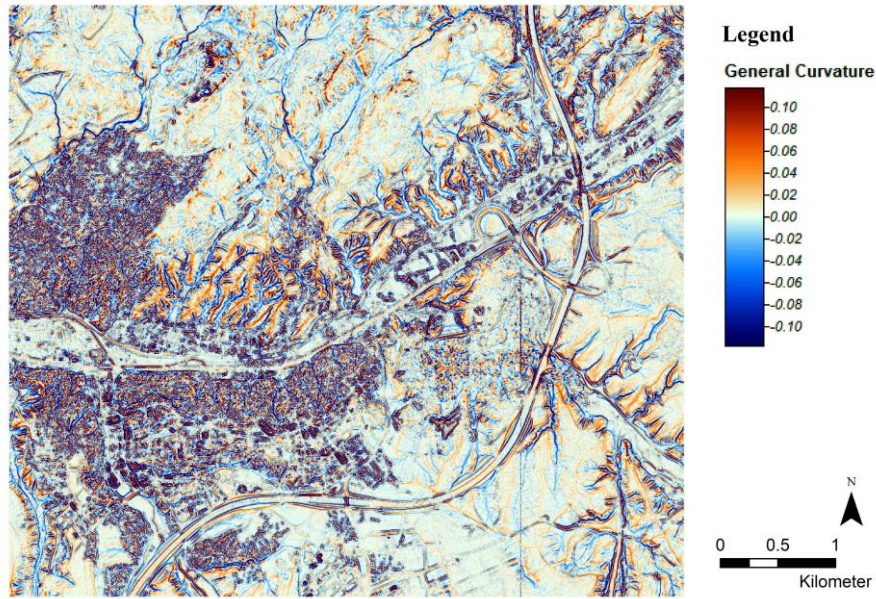


Figure 4.4. General curvature map.

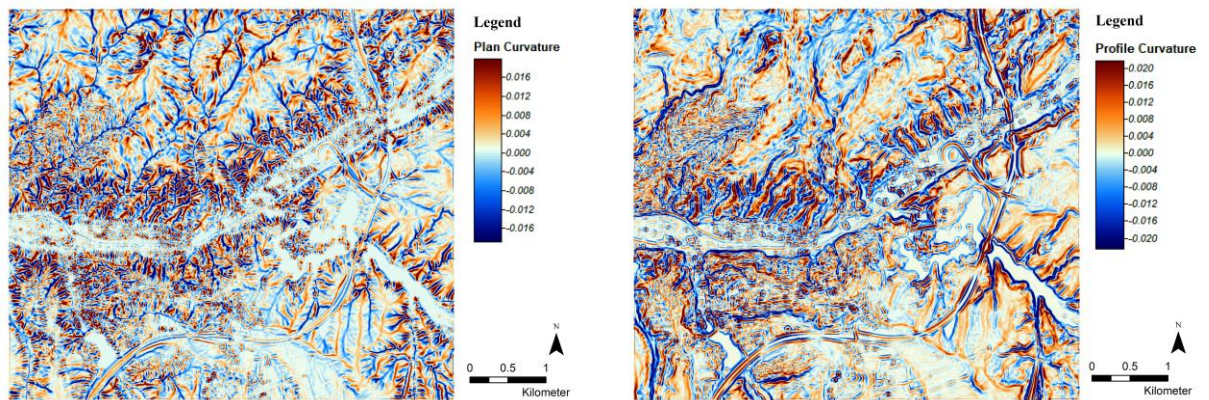


Figure 4.5. Plan and profile curvatures maps.

4.2.1.4. SPI and TWI

SPI shows the rate of the corrosive power of the flowing water [92] and denotes potentiality of sediments' erosion power, thus, it is efficient for LS assessment [93] (Figure 4.6). This factor displays flow conditions with a moderate level of abrasion concerning the sudden alterations in topography and steep slopes [88]. SPI is calculated using the flowing formula [87]:

$$SPI = A_s \times \tan \beta \quad (1)$$

Where;

A_s = specific catchment area

β = slope in degree.

Place and extent of the water-saturated regions are expressed as TWI in the topographical sense [80] (Figure 4.6). The infiltration of water into the material causes both pore water pressures in the material to increase and the strength of the material to decrease [88]. TWI is calculated using the following formula [87]:

$$TWI = \ln(A_s / \tan \beta) \quad (2)$$

Where;

A_s = specific catchment area

β = slope in degree.

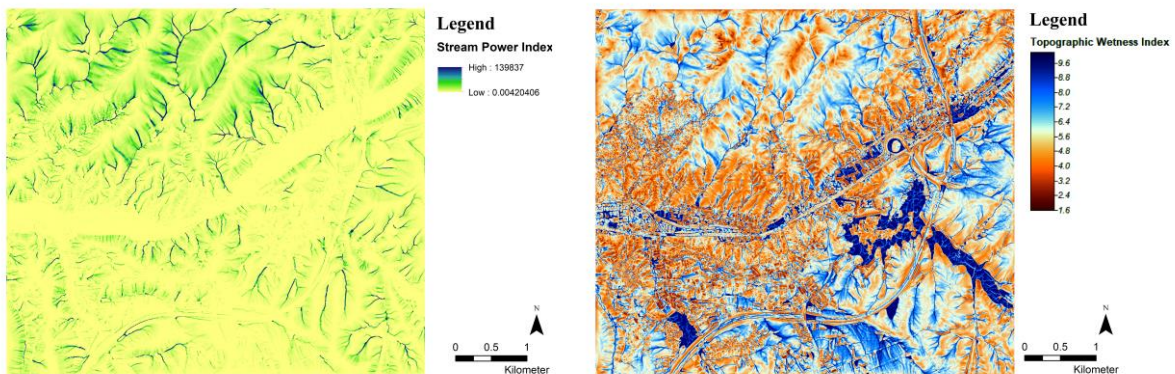


Figure 4.6. SPI map and TWI maps.

4.2.1.5. Breakline Proximity (Channels and Ridges)

The orthogonal distances to channels are used to notice landslides that happened near to a channel are detected with this parameter. DTM is used for computing vertical distances to the channel networks [94]. The channel proximity parameter had been evaluated in terms of its ability to affect stability negatively by eroding the surface or saturating the slope, or both [89]. Landslide occurrence possibility and distance to the ridgelines have a negative correlation for the same reason [90]. Flow direction and stream

network parameters were used for ridge computation. Then the distances to the ridgelines were calculated. Euclidean distance to both channels and ridgelines were produced by FME Software. Both distance maps to the ridgelines and channels are presented in Figure 4.7.

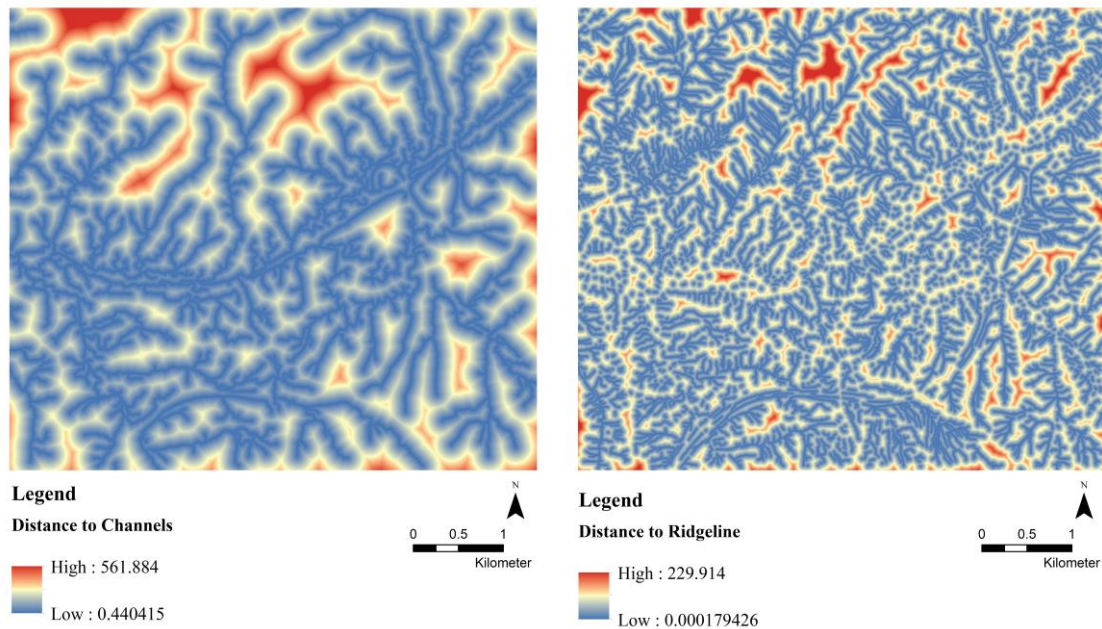


Figure 4.7. Proximity to channels and ridgelines.

4.3. Image Classification with Random Forest Method

LULC data's currency and accuracy is necessary for natural hazard assessment and hazard reduction purposes. Sentinel-2 images with 10-m GSD was used to generate LULC data in this study. 13 bands of Sentinel-2 satellite images were used for classification and the contributions of bands other than RGB bands was found very little. This situation varies depending on the site characteristics. The other bands have the potential to provide advantages for other study areas with different characteristics. In this thesis, RGB bands are processed using SNAP software to obtain seven LULC classes. Training data on the images were collected for supervised classification. RF method was used for this purpose. A cluster of decision trees generated by using trainings and variables for image classification using the RF method [95]. Pixels that have maximum rates from all trees are classified in the decision trees. Many ML methods are used for image classification but RF has importance among these because of its higher accuracy on image classification [96-99]. Furthermore, as argued in Lim et al. [100], the RF method

is useful with high accuracy on Sentinel-2 images. The numbers of trees and variables are the main parameters for the RF classifier [101].

Image classification was performed by building 10 trees and using 2077 training samples on three bands, i.e. RGB and processed GLCM-ASM (Gray-Level Co-Occurrence Matrix Angular Second Moment) in this study. The Gray Level Co-occurrence Matrix (GLCM), which shows the measure of surface textures, improved classification accuracy. There were industrial areas and roads that had similar brightness values in the satellite image with only RGB bands. Therefore, industry areas were classified under the heading road/rail networks/associated land. As suggested by Stumpf and Kerle [102], GLCM values were computed in all directions and used to improve classification accuracy. Among the GLCM parameters, Angular Second Moment (ASM) parameter had a visible contribution to the determination of industrial areas in this study.

4.4. LS Map Generation with LR Method

Several mathematical and ML techniques can be utilized for LS map generation. In the literature, there are numerous research on the estimation of LS using LR (e.g., References [103–108]). Multivariate LR was chosen to produce the LS pattern in the test site. Because of its fast and precise working potential for the LS assessment, LR is one of the analytical models used to predict the potential landslide zones in this study [9, 90, 109]. LR is working with dependent and independent variables. A binary map that describes landslide potential is used as dependent variable [92]. Generated landslide conditioning factors like elevation data, slope, LULC, lithology, etc. were used as independent variables. The correlation between dependent and independent variables using landslide inventory and non-landslide samples chosen at random was analyzed for the potential risk estimation in the LR model. The logistic regression model is computed with equations (3) and (4).

$$Y_i = \beta_0 + \beta_1 X_i \quad (3)$$

$$P_i = (Y = 1|X_i) = 1/(1 + e^{-Y_i}) \quad (4)$$

Where;

Y_i describes the dependent variable,

X_i describes the independent variables,

β_0 is a constant,

β_i presents the i -th regression coefficient,

P_i is the probability of the presence of landslides [90].

In the literature, many studies like Vorpahl et al.'s [110] and Park et al.'s [111] worked on creating LS maps using similar factors as here, and it is concluded that the most precise method was LR compared with other methods. Here, the LS map of the whole site was produced after determining LR model, which were computed with samples having 1:2 ratio. In other words, approximately 2000 grid points were used for landslides and approximately 4000 grid points were used for non-landslides.

4.5. MHS Assessment

Mamdani Fuzzy Algorithm (MFA) [112] is used for creating a MHS assessment map by combining flood and landslide susceptibility maps. "if-then" rules are used for resolving complicated problems to defeat uncertainties in this method. Mamdani Fuzzy Inference System (Mamdani FIS) has four stages called fuzzification, rule evaluation, aggregation, and defuzzification [112]. Provided crisp inputs are used for generating crisp outputs by using a fuzzy set theory in FIS [113]. In the literature, there are various research about the general structure of a Mamdani FIS (i.e., References [114–117]). An integrated tool was produced for the development of a Mamdani FIS for Netcad Software, Netcad, Ankara, Turkey by Osna et al. [117]. The Mamdani fuzzy logic [118] operator in Netcad was used to evaluate both susceptibilities to generate MHS. The MFA was handled for LS mapping in the literature [116-117,119]. Yet, LS and FS maps are combined to get a MHS map in the current study as an initial attempt.

The multi-hazard susceptibility level (MHSL) is acquired from MFA that uses LS and FS maps as an input. A fuzzy model is produced by applying expert knowledge in the framework of linguistic rules. Figure 4.8 shows the membership functions and fuzzification stage of the system. Each input and output have three membership functions (low, moderate, and high) in the Mamdani FIS here. The membership degree is stated in the y-axes of the graphs, and the susceptibility levels are indicated in the x-axes. The

susceptibility levels change for landslide (between 0-1) and flood (between 8-66). Numerous techniques have been used for membership value assignment in previous researches, such as intuition, rank-ordering, angular fuzzy sets, genetic algorithms, inductive reasoning, soft partitioning, etc. (e.g., References [120–122]). A generic approach is used here to decide membership functions. Two inputs and one output are used for the constructed fuzzy model with three membership functions in this study. In addition, the fuzzification of crisp numbers and the membership degree of each crisp input were measured in this step. Developing the rule evaluation (linguistic if-then rules) is one of the key points of a Mamdani FIS. Prof. Dr. Candan Gökçeoğlu produced the if-then rules as the expert. This enabled the rules to be written without the need for extensive research. A total of 9 rules were created by the expert and shown in Table 4.3. The collection of all results from fuzzy rules triggered in the rule evaluation stage was used for creating the final fuzzy output of the model [117]. In the Mamdani FIS formed in this study (Figure 4.9), the max. operator was analyzed for aggregation, as recommended by Reference [117]. Lastly, defuzzification was done using the center of gravity. The LS and FS maps were employed for operating the Mamdani FIS formed. The MHSL map are shown in the next section.

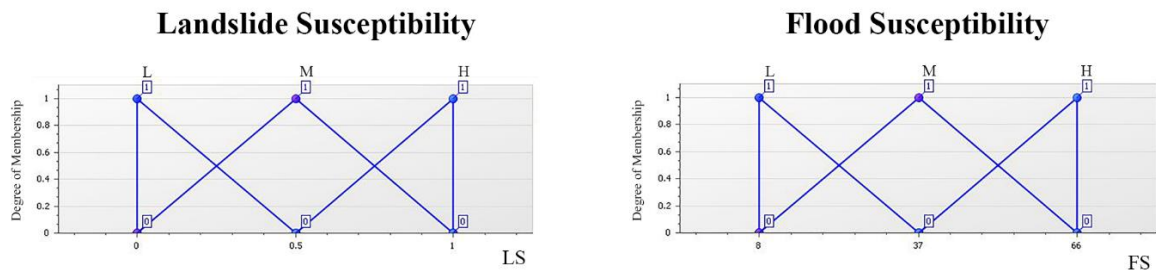


Figure 4.8. The membership functions of LS (on the left) and FS (on the right). The x- and y-axes show the susceptibility level interval and the degree of membership, respectively.

Table 4.3. Rule evaluation stage (if-then fuzzy rules) of the MHSL assessment.

RULE NO.	RULE
1	If (LS is high) and (FS is high), then (MHSL level is high)
2	If (LS is high) and (FS is moderate), then (MHSL is high)

3	If (LS is high) and (FS is low), then (MHSL is high)
4	If (LS is moderate) and (FS is high), then (MHSL is high)
5	If (LS is moderate) and (FS is moderate), then (MHSL is high)
6	If (LS is moderate) and (FS is low), then (MHSL is moderate)
7	If (LS is low) and (FS is high), then (MHSL is high)
8	If (LS is low) and (FS is moderate), then (MHSL is moderate)
9	If (LS is low) and (FS is low), then (MHSL is low)

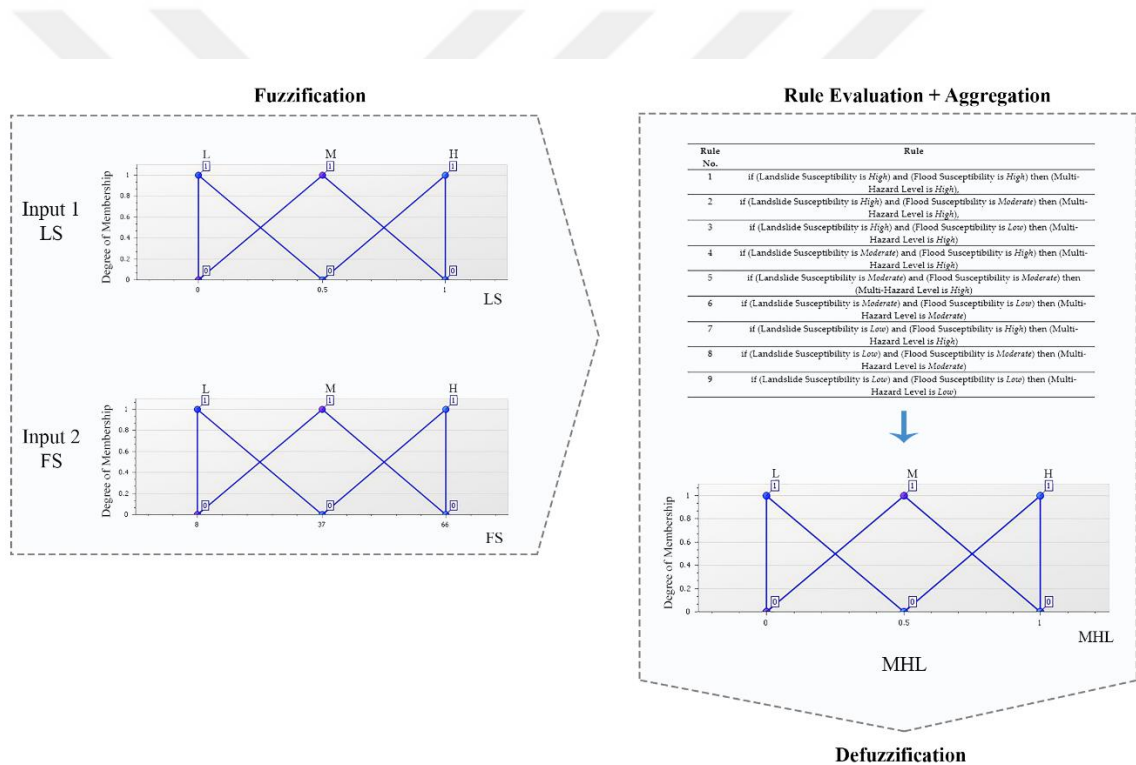


Figure 4.9. Overall framework of the Mamdani FIS constructed.

5. RESULTS

5.1. Image Classification Results

The LULC result obtained by SNAP software is shown in Figure 5.1. This classification includes seven important classes for urban land-use planning. Table 5.1 shows the dispersion of the training samples to the seven classes. The cross-validation technique was applied for the accuracy assessment of classification and results show that the true prediction rate, the classification accuracy, and the Kappa value are 93.73%, 92.01%, and 97.13% as shown in Table 5.1. While performing the classification, SNAP software automatically performed cross-validation according to internally defined rates. GLCM-ASM parameter increases the classification accuracies of all bands (Table 5.1). Although industrial units seem like have the same and high accuracy for both forms, it was mainly beneficial for separating the roads and the industrial units as a class.

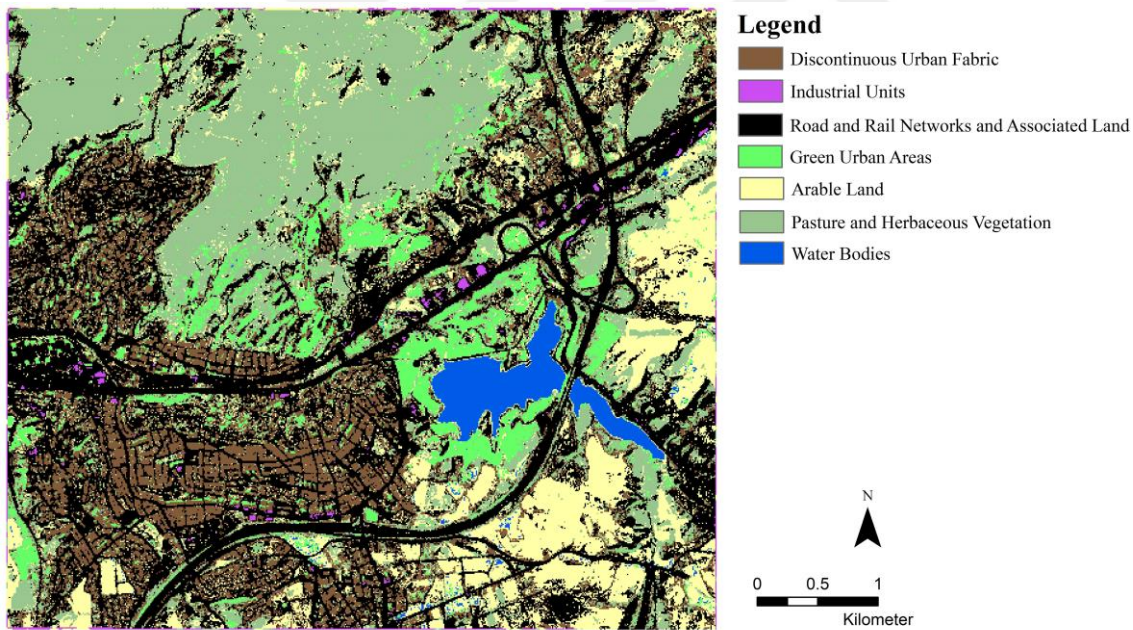


Figure 5.1. LULC map as a result of the image classification.

Table 5.1. Classification accuracy of the image classification with Random Forest method

Land Use	Number Of Training Samples	Classification Accuracy (Cross-Validation) (With GLCM-ASM)	Classification Accuracy (Cross-Validation) (Without GLCM-ASM)
Discontinuous Urban Fabric	401	98.75%	94.01%
Industrial Units	36	98.84%	98.94%
Road and Rail Networks and Associated Land	811	97.10%	94.4%
Green Urban Areas	146	99.71%	97.88%
Arable Land	325	98.75%	96.72%
Pasture and Herbaceous Vegetation	125	98.65%	96.14%
Water Bodies	233	99.81%	99.71%
Overall	2077	93.73%	83.11%
Kappa Coefficient		97.13%	93.68%

5.2. The Landslide Susceptibility Results

Figure 5.2 shows the LS map created here. Notwithstanding that the values of landslide accruing possibility changed between 1%–99% (i.e., from 0–1, the LS membership chart as given in Figure 4.8), equal interval classification was used for reclassifying values into three groups (low, moderate, and high) for clear understanding. They were also employed in the MFA. Current LS notably in the west of the study site was proved in this map. Expert opinions about the field confirm the outputs of the study.

For a better understanding of precision on the LS map, an accuracy assessment of the output was evaluated. The implemented methods, data quality, the number of inputs, and the strategy for map production had an impact on the accuracy of the output [84].

Figure 5.3 shows the accuracy with the ROC curve, an indicator of the used model's success on classification [123]. As it is understood from the curve, the LS map generated in this thesis exhibits 96% accuracy.

As mentioned in the previous section on the LS Map Generation with the LR Method, the regression coefficients were calculated for each parameter. The regression coefficients show the relationship between the parameters and the landslide formations [90]. The regression coefficients obtained for each landslide conditioning parameter are given in Table 5.2. According to the Table, while there is a positive correlation between slope, aspect, general curvature, plan curvature, SPI, TWI and LULC parameters that have positive landslide susceptibility values and landslide occurrence, there is a negative correlation between altitude, profile curvature, lithology and distance to channels and ridgelines parameters that have negative landslide susceptibility values and landslide occurrence.

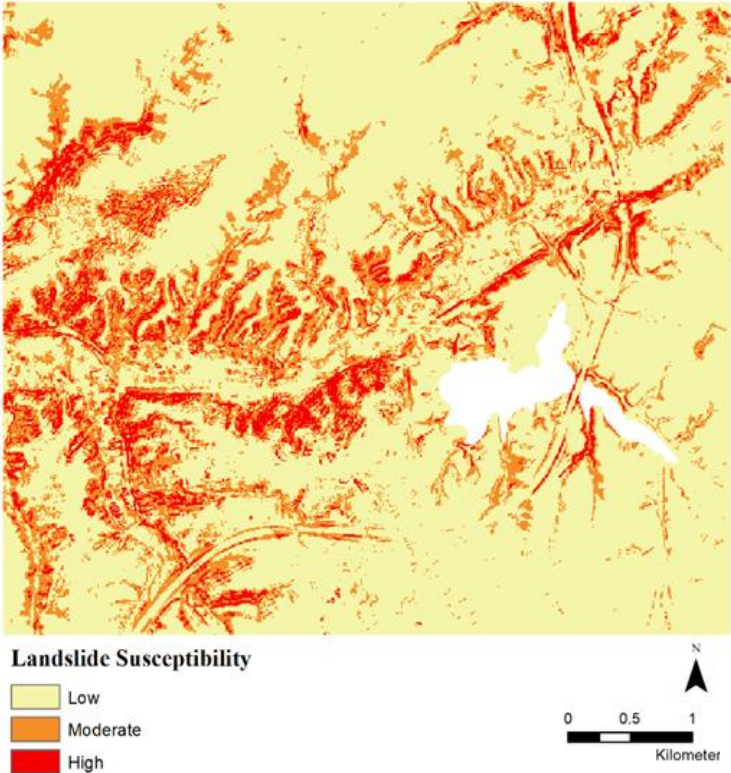


Figure 5.2. LS map obtained in this thesis.

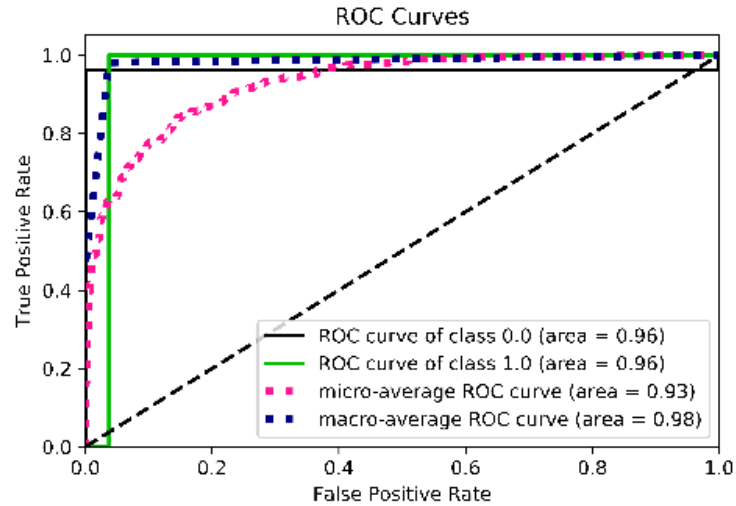


Figure 5.3. ROC curves of the LS map.

Table 5.2. Regression coefficients of the landslide conditioning parameters.

Parameters	<i>Altitude</i>	<i>Slope</i>	<i>Aspect</i>	<i>General Curvature</i>	<i>Plan Curvature</i>	<i>Profile Curvature</i>
Regression Coefficients	-0,0156	0,113	0,0043	0,346	0,329	-0,207
Parameters	<i>Distance to Channels</i>	<i>Distance to Ridgelines</i>	<i>SPI</i>	<i>TWI</i>	<i>Lithology</i>	<i>LULC</i>
Regression Coefficients	-0,00497	-0,0353	0,0000 03	0,0046	-0,156	0,0744

5.3. Multi-Hazard Susceptibility Results

Landslide and flood susceptibility maps were combined to form a multi-hazard map for the basis of urban planning. These two hazards affect each other and the flood event may trigger the landslide event. Thus, an effective methodology was recommended for combining several susceptibility maps in this study. The MHSL map, which was a result of the MFA, is generated (Figure 5.4). As an outcome, some of the hills and valleys in the study area suffer from high multi-hazard potential. Figure 5.4 displays regions which

have high MHS to reduce the damages of natural hazards. Also, the distribution rate of the MHSL is given in the Table 5.3. This output should be examined correctly, and in the urban transformation periods, construction decisions should be made carefully.

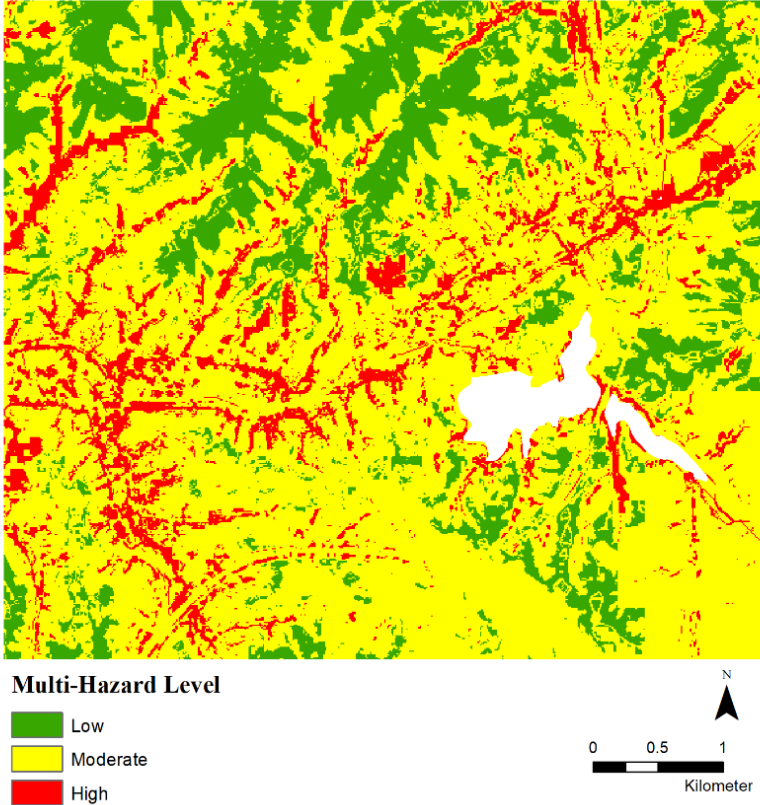


Figure 5.4. Multi-hazard susceptibility level map produced in this thesis.

Table 5.3. Distribution rates of the MHSL.

Multi-Hazard Level	Ratio
Low	21%
Moderate	67%
High	12%

5.4. Elements at Risk

Van Westen et al. [124] presented that further data needed for the evaluation of risk assessment involve elements at risk. Although these elements involve many factors (e.g. population, constructions, financial actions, municipal services, and utilities), as mentioned in the study, the most important elements are buildings, population, and infrastructure. This approach is also adopted in this thesis and it is aimed to calculate the percentages of the elements at hazard as a first attempt.

Therefore, the areas at high susceptibility were vectorized and superposed with the land use map created in this thesis (Figure 5.5). As a result of this overlay, the percentages of the elements at the highly susceptible areas is given in Table 5.4. As it is seen, the element at the highest risk is the road and rail networks and associated land one of the technical infrastructure elements. In addition, residential areas share 15% of the distribution is another element at risk that should be considered. In this regard, transport systems and settlements that are at multiple natural disaster risks are the points that should be given importance in urban projects.

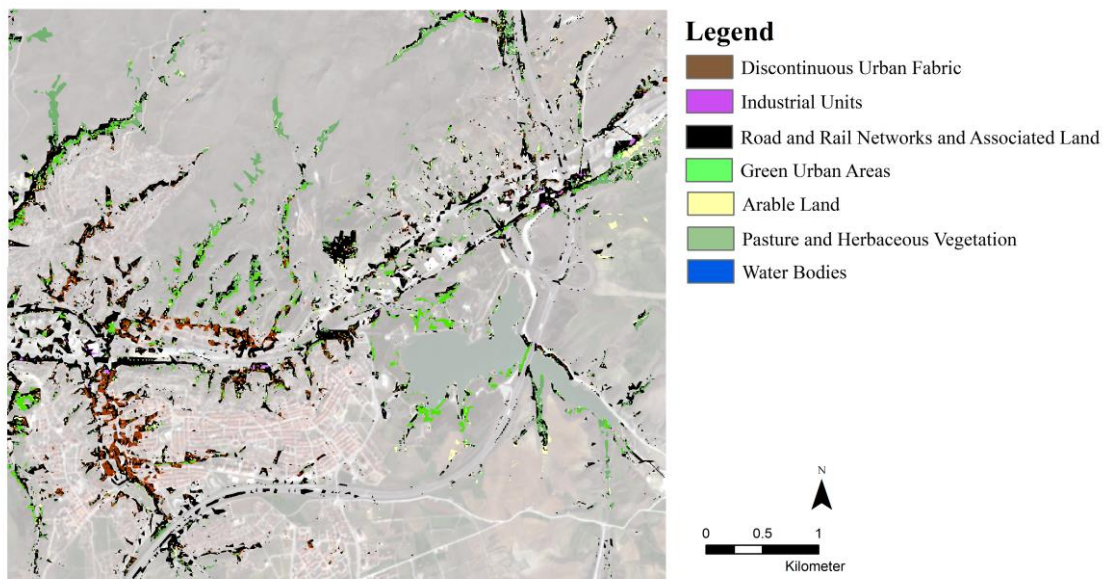


Figure 5.5. Multi-hazard susceptibility level map produced in this thesis overlaid with the LULC.

Table 5.4. Distribution rates of the land use classes at high MHSL areas.

Land Use	Ratio
Discontinuous Urban Fabric	15%
Industrial Units	1%
Road and Rail Networks and Associated Land	38%
Green Urban Areas	7%
Arable Land	18%
Pasture and Herbaceous Vegetation	21%
Water Bodies	0%

Also, vector drawings of the buildings and areas with the highest risk level in the study area were intersected to find out how many buildings are at the highest risk level. As a result, it was discovered that 2771 buildings are located in the area with the highest MHSL (Figure 5.6). The average number of households in the neighborhoods in the study area was calculated at 3.18 [125]. In this case, it was assumed that the number of households living in one building was 5, keeping the number low due to the presence of slum areas. According to the results, there are 44.058 people at high MHSL in the study area. Urban planning decisions to ensure the safety of life and property of these people should be taken by city planners.

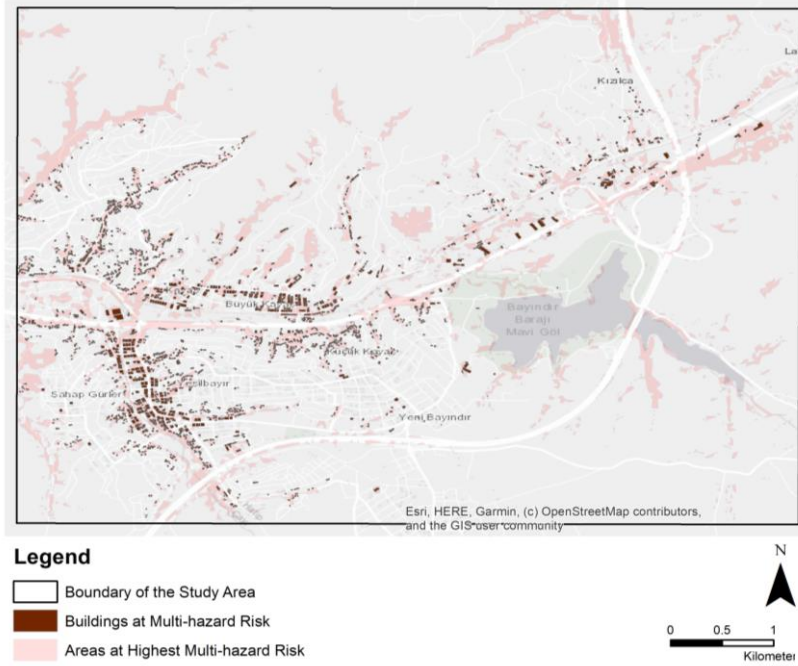


Figure 5.6. Buildings at the high MHSL areas.

6. DISCUSSIONS

6.1. Mamak Urban Transformation Plan

Due to the urbanization upgrowth of Turkey, rural to urban migration is increasing. In general, domestic immigrants coming from the eastern part of the country to Ankara were settled in Mamak District. For this reason, there is an unplanned settlement structure consisting of slums in common [126]. This situation caused the need for planned urbanization and for this purpose, then the New Mamak Urban Transformation Project was created [127]. Figure 6.1 shows boundaries of different implementation stages of the New Mamak Urban Transformation Project [126].



Figure 6.1. Boundaries of implementation stages of Mamak Urban Transformation Plan [126]

Mamak Urban Transformation Plan includes 13 neighborhoods which are Derbent, Dostlar, Araplar, Köstence, Dutluk, Şirintepe, Yeşilbayır, Fahri Korutürk, Üreğil, Büyükkayaş, Küçükkayaş, Tepecik, Şahap Gürler. The aim of the project is explained as preventing slum building in Mamak, creating proper structures suitable for zoning and giving the city an aesthetic area [127]. There are 13.497 squatter houses in the

project area and 5.340 houses was already demolished. The study area includes Küçükkayaş, Yeşilbayır, Şahap Gürler, Büyükkayaş neighborhoods and some parts of Üreğil, Dostlar, Tepecik and Köstence neighborhoods. This project is planned to complete in 11 stages. (Figure 6.2) The total number of dwellings delivered at these stages, under construction or at the project approval stage has reached to the number 5,150. In this direction, the production of 5,150 houses, 2,358 units in Stage 1, 1,181 in Stage 4, 1,150 in Stage 5, and 461 in Stage 6, has been completed [126]. Total population of the project area is 56.000 but it is planned to serve for 200.000 people. Yeşilbayır, which is a most populated neighborhood in Mamak, is located in the study area. This situation supports importance of resilient urban transformation plan need.

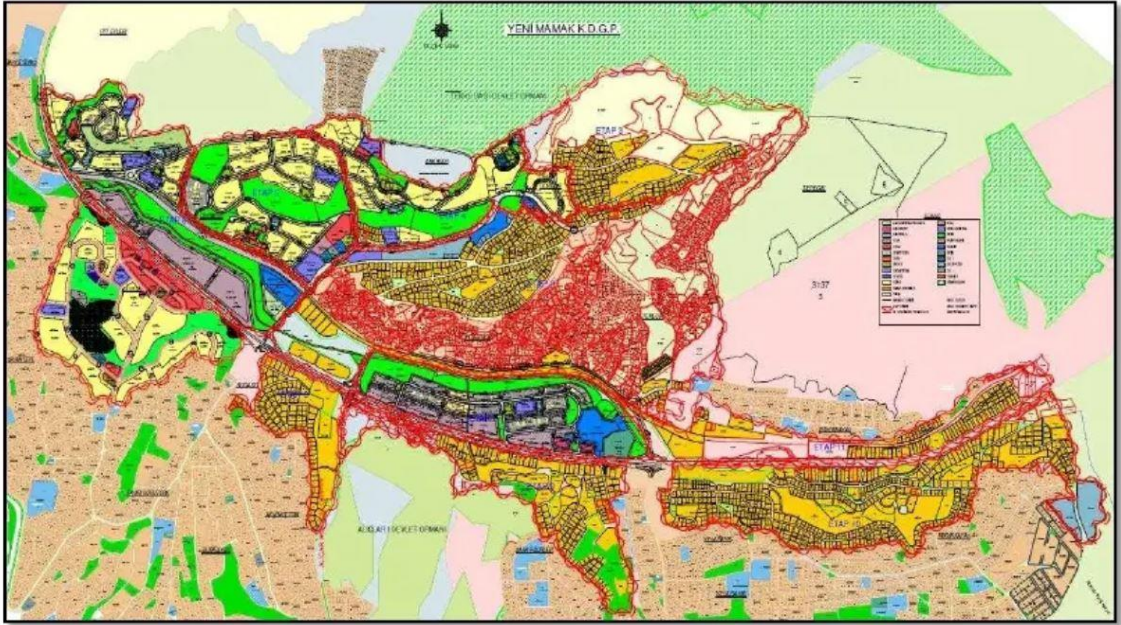


Figure 6.2. Mamak Urban Transformation Plan [126]

When the MHS assessment map produced in the study and project areas are superposed, it can be seen that the project includes most of the highly susceptible areas. Accordingly, the necessary measures should be taken in the new settlements' resistance to these risks. For instance, although there are few completed transformations within the study area, it was seen that most of the buildings are high-rise (14-15) when the completed project stages were reviewed (Figure 6.3). The durability of these houses in any disaster situation may need to be tested.



Figure 6.3. A completed stage of Mamak Urban Transformation Project [127].

According to Cutter [128], general concepts that should be calculated for community disaster resilience are examined under two headings as assets (economic, social, environmental, infrastructure) and capacities (social capital, community functions, connectivity, and planning). Yeşilbayır, Küçükkayaş and Dostlar districts located at the junction of risky areas and transformation should be examined within the framework of these headings.

In general, areas belonging to the urban transformation project are at a moderate MHSL. Therefore, the locations of the buildings at risk in the existing project should be determined and the durability of these areas in the project result should be recalculated. The susceptible areas of this project need to be reviewed.

6.2. 3D Models of Results

For an exposition of the outcomes, 3D models of the DEM overlaid with the Sentinel-2 image (Figure 6.4), the LS map (Figure 6.5), the FS map (Figure 6.6), and the MHSL map (Figure 6.7) were visualized with the QT Modeler tool [129].



Figure 6.4. The digital terrain model that has a textured surface with the Sentinel-2 image.

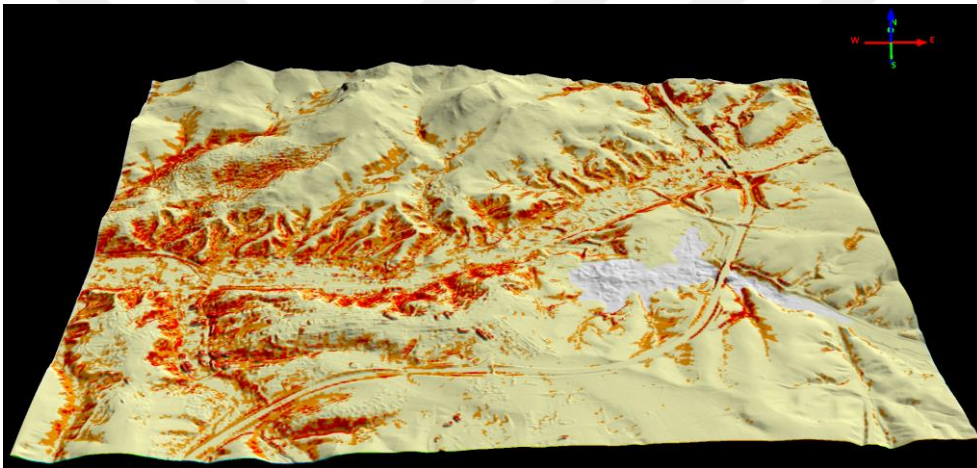


Figure 6.5. The DTM that has a textured surface with LS map (result of LR method).

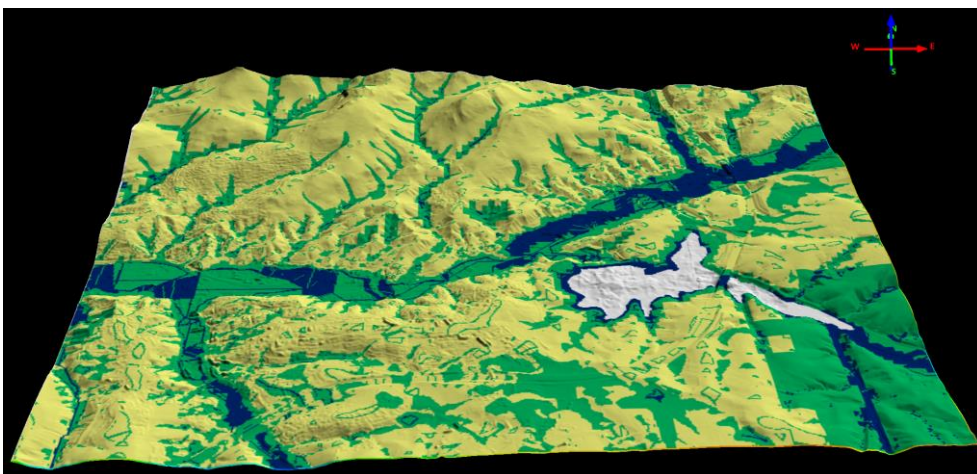


Figure 6.6. The digital terrain model that has a textured surface with the FS map.

There are some points to be considered in the urban transformation project. (Figure 6.7) For example, there is low LS, high FS and moderate-high MHS in the pink circle in Figure 6.7. As mentioned before, the current flood and landslide resistance of this transformation-completed area should be considered.

There are many slums in the Mamak region. It is concluded that many of these are in the MHS areas. These areas are indicated by green circles in Figure 6.7. In these areas, it is more convenient to make agreements with property owners, to develop certain policies and to increase the use of urban green areas. Newly built buildings in this area (dark-blue circle in Figure 6.7) are also at risk. These areas should not be neglected relying on buildings' age and the conditions under which they are renovated should be examined. Another point that draws attention in this circled area is that Sağduyu Caddesi, which is a trading axis, is a completely at-risk area. The activity of the commercial area within the risk should also be examined. Another issue is the industrial area at risk (purple circle in Figure 6.7), as mentioned in the previous sections.

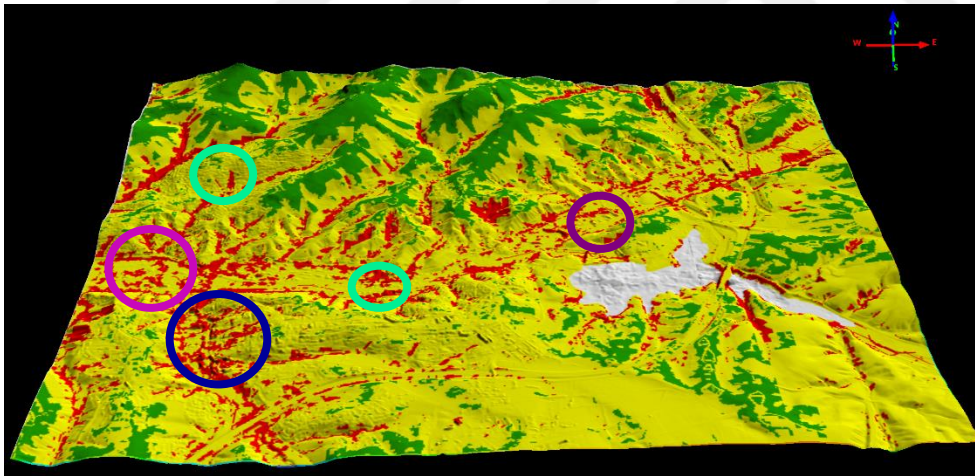


Figure 6.7. The digital terrain model that has a textured surface with the MHS map. The rings indicate significant focal spaces for urban planning in North-West and South Mamak as discussed before.

Concerning the methodological approach applied in this thesis, the precision of the LR technique was found sufficient. Despite the small amount of training data, using two non-landslide pixels for every landslide pixel operated effectively. The MHS map represented the objectives, and can be accepted as a basemap for some city planning

projects. The LR and M-AHP methods used for LS and FS maps were valuable, and the MFA was powerful to determine the MHSL.

6.3. Urban Risk Management

While natural hazards are generally expressed as unpreventable, these hazards turn into disasters only when the coping mechanisms of the related communities are exceeded and these communities cannot manage the effects of disasters [130]. In Turkey, partial reasons for the excessive damages in natural disasters are the lack of integration between disaster and urban development laws [131-132]. Yet, in the past twenty years, the policies have not been limited to only post-disaster relief. So, this is the transition from a fatalist society to a self-relying society in urban planning. According to Balamir [133], while fatalist societies attach importance to post-disaster recovery strategies, improvement efforts, and crisis planning; risk societies attach importance to prevention strategies, preparatory works, and contingency planning. All of them are based on the awareness that efforts and investments will effectively serve to reduce losses in the event of any natural hazard. When both administration approaches are considered as important; and the risk management, emergency management, and post-disaster crisis management are evaluated together, the ability to cope with natural hazards also increases.

With these changes, the research studies on determining the risks and possible losses before natural hazards; and systematically eliminating, reducing, and sharing the risks have come to the fore [134]. The risks posed by natural hazards can be avoided if the underlying causes of the events can be known and appropriate mitigation approaches can be implemented. This is called risk management (pre-disaster) rather than disaster management (post-disaster) [131]. In addition, risk management can be provided through urban mitigation plans. The main topics that can be used for effective risk management are avoidance, minimization, and sharing [131]. Briefly, the outputs produced in this thesis also have the potential to be used in the risk management phase.

In the risk avoidance header, which is an important part of risk management, it is necessary to avoid the selection of areas under risk for settlement intentions, to determine the minimum distance to be avoided from points in high risk, and to make planning decisions by taking into account the triggering situations of disasters determined by multi-hazard maps [131]. In short, the most important method of avoiding risk is making correct

land-use decisions. However, even if the risks are minimized with the implementation of these actions, the risks cannot be eliminated. In this case, it is necessary to move on to minimize the risk. Here, to minimize the risks, it is necessary to ensure the sufficiently robust design of the buildings, increase the on-site resistance of the buildings, or rejecting risks at source like flood-control reservoirs [131]. All these measures will ensure that sharing the effects of risk on society and funding for pre-disaster and post-disaster needs.

The Mamak region is under enormous development pressure as part of urban sprawl. In this case, the evaluation of natural hazard susceptibility is essential in development plans made or to be made. Steps that are taken to ensure risk management will contribute to the formation of more resilient urban parts. In summary, the areas under high natural hazard susceptibility determined by using the maps produced in the thesis can be evaluated in these stages and a connection can be established between disaster and development laws.

7. CONCLUSIONS AND FUTURE WORK

7.1. Conclusions

A fuzzy model was produced to evaluate landslide and flood susceptibility maps collectively in this thesis. Another focus of this study in which many methods are used is to obtain actual LULC data to be employed in the generation of a LS map using Sentinel-2 satellite images. This data was created by the Random Forest classification technique. The quality of the created LULC classes was increased by adding the GLCM-ASM parameter. With the contribution of the ASM parameter, the correct classification of roads and industrial areas has been ensured. As a result, the usability of Sentinel-2 satellite images in land use map generation in urban development areas was evaluated and found adequate for the purposes of the study. The extraction of topographic parameters required for the generation of LS maps was made using the high-resolution DEM. Production of LS map using topographic parameters, lithology data, and LULC data was completed with the LR method. FS map was obtained from the study of Sozer et al. [19-20]. MHS assessment was produced using these two susceptibility maps. MFA was used in the production of the MHSL map.

The principal complication faced throughout the research was the generation of a completely formed landslide inventory map because of the high urbanization level. Yet, a unified methodology was developed and featly implemented to produce the MHSL map.

In the international literature, the methodology developed in the thesis is the initial in the generation of MHS maps. The outcomes of combining landslide and flood susceptibility maps using the expert-based fuzzy inference method were highly favorable. Thesis results also demonstrate that Mamdani FIS is a proper method for MHS assessment. Yet, an appropriate methodology is not existent for the accuracy assessment of MHS maps. Since this was foreseen at the beginning of the study, the study zone was chosen from a small and well-recognized region. As a result, the ultimate map was evaluated with expert knowledge.

Consequently, the fuzzy algorithm introduced for MHS assessment has an adaptable and simple working principle. Therefore, if further data is acquired, this model can be effortlessly modified and reconfigured.

It has been observed that the planning decisions to be made depending on the multi-hazard susceptibility map produced in this thesis can contribute to risk management. Percentages of the elements in high exposure were calculated, the number of structures and population were estimated. It was observed that the decision making processes of the governments in risk avoidance and mitigation activities will accelerate with these outcomes. The results can be used to form the decisions to be taken in 1/1000 and 1/5000 scale master plans within the concept of urban resilience, which are remarkably important for city planning.

Although it is necessary to know the existing construction and land use conditions in detail in order to determine the risk rank in the hazardous areas, generally the following stages need to be carried out;

- to determine the resilience of the infrastructure (transportation, communication, etc.) and to improve it in case of deficiency,
- to create alternative transportation/access options for possible hazards,
- to make road network improvements and expansions,
- to examine the vulnerability level of the population by making detailed examinations on buildings and repositioning them temporarily/permanently or minimizing the effects of risk for that population by making on-site improvements,
- to determine the drafts on growth and displacement/selection of large areas such as industrial areas,
- to carry out fund, worker and material planning,
- if risky areas are not in the built environment, to use of building designs that will ensure the resistance of the structures to possible hazards in case of any construction, or to use these areas as open spaces,
- if risky areas are in the built environment, to test the durability of the buildings with different parameters and to strengthen the buildings on-site, or to reposition the households and providing the required urban transformations without harming the households socially or economically,

- to re-evaluate the open and green areas and increase this type of use in risky areas,
- to reassess the decisions in the urban transformation plan within the framework of urban resilience etc.

All these actions can be developed, modified, and regulated by city planners by examining multi-hazards and city structures together in a specific area. It is not possible to argue about precise decisions at this stage, because no structure-based information about the area has been collected.

7.2. Future Works

Urban planning decisions should be made very accurately in areas at high risk in the MHSL map. Development in the existing urban transformation plan should be evaluated accordingly or, if feasible, the construction in these areas should be minimized and loss of life and property should be abstained. Maps created with this aspect are likely to be used in city planning. In the plans used by these maps as a base, it is possible that the advantages provided in the social, economic and political sense may emerge in the long term. The use of the Mamdani FIS method in the collective assessment of natural disasters may also give new opportunities and supports in the land suitability analysis. The MHSL map created in the test site area, which is currently under urban transformation projects, has the potential to be used as an important resource for urban planning. For this purpose, analysis can be extended in future studies to be used in planning stages.

Also, in future studies, some efforts should be made for performance evaluations in joint assessments of natural hazards and some mathematical methods should be produced for precision.

It is not enough to identify the hazardous areas in the cities. The main topics such as macro form, urban texture, land use, infrastructure, structure stock analysis, and urban management, and operational insufficiencies should be reviewed with natural hazard susceptibility assessment in urban planning. Additionally, in future studies, a damage estimation can be created based on the elements at risk that are identified in the thesis and by adding detailed information (e.g. quality of buildings, building age, construction year, building material, durability of the structure, socio-economic situation). This damage

estimation will have the potential to become an important resource that will affect and shape city planning policies.

As a fair sample of transforming multi-hazard assessment to multi-risk assessments, the study from Barria et al. [135] can be reviewed. In this study, the multi-hazard susceptibility map created with the common evaluation of landslide, flood, and earthquake combined with the characteristics of settlements, social and technical infrastructures for the risk assessment. As a result, a relationship matrix was created between a vulnerability rate and a multi-hazard degree. In this case, a general multi-risk map has been obtained by evaluating the hazards with the matrices of socio-economic and physical vulnerability values of the study area. As mentioned in this study, output results were used to create an urban mitigation plan and urban planning decisions about the resilient settlement were made for the study area. Similar to the study of Barria et al. [135], the next stage of this thesis is the multi-risk assessment that will be carried out by processing these features and the conversion of this into policies that will be the basis of an urban mitigation plan.

6. REFERENCES

1. Kocaman, S., Anbaroglu, B., Gokceoglu, C. and Altan, O., A review on citizen science (CitSci) applications for disaster management. *International Archives of the Photogrammetry, Remote Sensing & Spatial Information Sciences; Geoinformation for Disaster Management (Gi4DM)*, Istanbul, Turkey, 2018, Volume XLII-3/W4, **2018**, pp. 301-306.
2. Mulero, D. L., Nja, O. and Fernandez, C. L., Landslide Risk Management in the Urban Development of Sandnes (Norway). *The International Archives of the Photogrammetry, Remote Sensing and Spatial Information Sciences; Geoinformation for Disaster Management (Gi4DM)*, Istanbul, Turkey, 2018, Volume XLII-3/W4, **2018**, pp. 327-334.
3. Kocaman, S. and Gokceoglu, C., On the Use of Citsci and VGI in Natural Hazard Assessment. *International Archives of the Photogrammetry, Remote Sensing & Spatial Information Sciences; ISPRS TC V Mid-term Symposium “Geospatial Technology – Pixel to People”*, Dehradun, India, 2018, Volume XLII-5, **2018**, pp. 69-73.
4. Yanar, T., Kocaman, S. and Gokceoglu, C., On the Use of Sentinel-2 Images And High Resolution DTM For Landslide Susceptibility Mapping in a Developing Urban Settlement (Mamak, Ankara, Turkey). *International Archives of the Photogrammetry, Remote Sensing & Spatial Information Sciences; Geoinformation for Disaster Management (Gi4DM)*, Prague, Czech Republic, 2019, Volume XLII-3/W8, **2019**, pp. 469–476.
5. AFAD. Afet ve Acil Durum Yönetimi Başkanlığı. <https://www.afad.gov.tr/> (Last Access: 1 December 2019).
6. Nefeslioglu, H.A., San, B.T., Gokceoglu, C. and Duman, T.Y., An assessment on the use of Terra ASTER L3A data in landslide susceptibility mapping: *International Journal of Applied Earth Observation and Geoinformation*, 14 (1) (**2012**) 40-60.
7. Pham, B.T., Shirzadi, A., Tien Bui, D., Prakash, I. and Dholakia, M., A hybrid machine learning ensemble approach based on a radial basis function neural

- network and rotation forest for landslide susceptibility modeling: a case study in the Himalayan area, India: *International Journal of Sediment Research*, 33 (2018) 157-170.
8. Gorum, T., Gonencgil, B., Gokceoglu, C. and Nefeslioglu, H.A. Implementation of reconstructed geomorphologic units in landslide susceptibility mapping: The Melen Gorge (NW Turkey): *Natural Hazards*, 46 (3) (2008) 323-351.
 9. Reichenbach, P., Rossi, M., Malamud, B. D., Mihir, M. and Guzzetti, F., A review of statistically-based landslide susceptibility models: *Earth-Science Reviews*, 180 (2018) 60–91.
 10. Sevgen, E., Kocaman, S., Nefeslioglu, H.A. and Gokceoglu, C., A novel performance assessment approach using photogrammetric techniques for landslide susceptibility mapping with logistic regression, ANN and random forest: *Sensors*, 19 (2019) 3940.
 11. Kocaman, S. and Gokceoglu, C., A CitSci app for landslide data collection: *Landslides*, 16(3) (2019) 611-615.
 12. Chen, L., Guo, Z., Yin, K., Shrestha, D. P. and Jin, S., The influence of land use and land cover change on landslide susceptibility: A case study in Zhushan Town, Xuanen County (Hubei, China): *Natural Hazards and Earth System Sciences Discussions*, 2019.
 13. Adhikari, P., Hong, Y., Douglas, K.R., Kirschbaum, D.B., Gourley, J., Adler, R. and Brakenridge, G.R., A digitized global flood inventory (1998–2008): compilation and preliminary results: *Natural Hazards*, 55 (2010) 405-422.
 14. CRED. Natural Disasters 2017, https://cred.be/sites/default/files/adsr_2017.pdf (Last Access: 1 December 2019)
 15. Gökçe, O., Özden, Ş. and Demir, A., Türkiye’de Afetlerin Mekansal ve İstatistiksel Dağılımını Afet Bilgileri Envanteri. Bayındırlık ve İskân Bakanlığı, Ankara, 2008. (in Turkish)

16. Perucca, L.P. and Angileri, Y.E., Morphometric characterization of del Molle Basin applied to the evaluation of flash floods hazard, Iglesia Department, San Juan, Argentina: *Quaternary International*, 233 (2011) 81-86.
17. Scheuer, S., Haase, D. and Meyer, V., Towards a Flood Risk Assessment Ontology - Knowledge Integration Into a Multi-Criteria Risk Assessment Approach: *Computers, Environment and Urban Systems*, 37 (2013) 82–94.
18. Cunha, N., Magalh, M., Domingos, T., Abreu, M. and Küpfer, C., The land morphology approach to flood risk mapping: an application to Portugal: *Journal of Environmental Management*. 193 (2017) 172-187.
19. Sozer, B., Kocaman, S., Nefeslioglu, H. A., Firat, O. and Gokceoglu, C., Preliminary Investigations on Flood Susceptibility Mapping in Ankara (Turkey) Using Modified Analytical Hierarchy Process (M-AHP). *International Archives of the Photogrammetry, Remote Sensing and Spatial Information Sciences*, 2018, p. 361-365.
20. Sözer, B., Kocaman, S., Nefeslioğlu, H. A., Firat, O. and Gökçeoğlu, C., Değiştirilmiş AHP (M-AHP) Yöntemi Kullanılarak Ankara İçin Taşkın Duyarlılık Haritası Üretimi: *Harita Dergisi*, 162 (2019) 12-24.
21. Nefeslioglu, H.A., Sezer, E.A., Gokceoglu, C. and Ayas, Z., A Modified Analytical Hierarchy Process (M-AHP) approach for decision support systems in natural hazard assessments: *Computers & Geosciences*, 59 (2013) 1-8.
22. Jaboyedoff, M., Oppikofer, T., Abellán, A., Derron, M.-H., Loye, A., Metzger, R. and Pedrazzini, A., Use of LIDAR in landslide investigations: a review: *Natural Hazards*, 61(1) (2010) 5–28.
23. Colesanti, C. and Wasowski, J., Investigating landslides with space-borne Synthetic Aperture Radar (SAR) interferometry: *Engineering Geology*. 88(3-4) (2006) 173–199.
24. Chen, W., Li, X., Wang, Y., Chen, G. and Liu, S., Forested landslide detection using LiDAR data and the random forest algorithm: A case study of the Three Gorges, China: *Remote Sensing of Environment*, 152 (2014) 291–301.

25. Weirich, F. and Blesius, L., Comparison of satellite and air photo based landslide susceptibility maps: *Geomorphology*. 87(4) (2007) 352–364.
26. Yao, X., Tham, L.G. and Dai, F.C., Landslide susceptibility mapping based on Support Vector Machine: A case study on natural slopes of Hong Kong, China: *Geomorphology*, 101 (2008) 572-582.
27. Brenning, A., Spatial prediction models for landslide hazards: review, comparison and evaluation: *Natural Hazards and Earth System Science*, 5(6) (2005) 853–862.
28. Pradhan, B., A comparative study on the predictive ability of the decision tree, support vector machine and neuro-fuzzy models in landslide susceptibility mapping using GIS: *Computers & Geosciences*, 51 (2013) 350–365.
29. Yesilnacar, E. and Topal, T., Landslide susceptibility mapping: A comparison of logistic regression and neural networks methods in a medium scale study, Hendek region (Turkey): *Engineering Geology*, 79(3-4) (2005) 251–266.
30. Pradhan, B. and Lee, S., Landslide susceptibility assessment and factor effect analysis: backpropagation artificial neural networks and their comparison with frequency ratio and bivariate logistic regression modelling: *Environmental Modelling & Software*, 25(6) (2010) 747–759.
31. Lee, S., Ryu, J.-H., Won, J.-S. and Park, H.-J., Determination and application of the weights for landslide susceptibility mapping using an artificial neural network: *Engineering Geology*, 71(3-4) (2004) 289–302.
32. Pourghasemi, H. R., Pradhan, B. and Gokceoglu, C., Application of fuzzy logic and analytical hierarchy process (AHP) to landslide susceptibility mapping at Haraz watershed, Iran: *Natural Hazards*, 63(2) (2012) 965–996.
33. Yalcin, A., GIS-based landslide susceptibility mapping using analytical hierarchy process and bivariate statistics in Ardesen (Turkey): Comparisons of results and confirmations: *CATENA*, 72(1) (2008) 1–12.
34. Yalcin, A., Reis, S., Aydinoglu, A. C. and Yomralioglu, T., A GIS-based comparative study of frequency ratio, analytical hierarchy process, bivariate statistics and logistics regression methods for landslide susceptibility mapping in Trabzon, NE Turkey: *CATENA*. 85(3) (2011) 274–287.

35. Fell, R., Corominas, J., Bonnard, C., Cascini, L., Leroi, E. and Savage, W. Z., Guidelines for landslide susceptibility, hazard and risk zoning for land use planning: *Engineering Geology*, 102(3-4) (2008) 85–98.
36. Hong, H., Tsangaratos, P., Ilija, I., Liu, J., Zhu, A.-X. and Chen, W., Application of fuzzy weight of evidence and data mining techniques in construction of flood susceptibility map of Poyang County, China: *Science of The Total Environment*. 625 (2018) 575–588.
37. Tehrany, M. S., Jones, S. and Shabani, F., Identifying the essential flood conditioning factors for flood prone area mapping using machine learning techniques: *CATENA*. 175 (2019) 174–192.
38. Khosravi, K., Pham, B. T., Chapi, K., Shirzadi, A., Shahabi, H., Revhaug, I., ... Tien Bui, D., A comparative assessment of decision trees algorithms for flash flood susceptibility modeling at Haraz watershed, northern Iran: *Science of The Total Environment*. 627 (2018) 744–755.
39. Tien Bui, D., Khosravi, K., Shahabi, H., Daggupati, P., Adamowski, J. F., M.Melesse, A., ... Lee, S., Flood Spatial Modeling in Northern Iran Using Remote Sensing and GIS: A Comparison between Evidential Belief Functions and Its Ensemble with a Multivariate Logistic Regression Model: *Remote Sensing*, 11(13) (2019) 1589.
40. Chapi, K., Singh, V. P, Shirzadi, A., Shahabi, H., Bui, D. T., Pham, B. T. and Khosravi, K., A novel hybrid artificial intelligence approach for flood susceptibility assessment: *Environmental Modelling & Software*, 95 (2017) 229–245.
41. Lee, S., Kim, J.-C., Jung, H.-S., Lee, M. J. and Lee, S., Spatial prediction of flood susceptibility using random-forest and boosted-tree models in Seoul metropolitan city, Korea: *Geomatics, Natural Hazards and Risk*, 8(2) (2017) 1185–1203.
42. Khosravi, K., Pourghasemi, H. R., Chapi, K. and Bahri, M., Flash flood susceptibility analysis and its mapping using different bivariate models in Iran: a comparison between Shannon's entropy, statistical index, and weighting factor models: *Environmental Monitoring and Assessment*, 188(12) (2016).
43. Razavi Termeh, S. V., Kornejady, A., Pourghasemi, H. R. and Keesstra, S., Flood susceptibility mapping using novel ensembles of adaptive neuro fuzzy

- inference system and metaheuristic algorithms: *Science of The Total Environment*, 615 (2018) 438–451.
44. Basheer Ahammed, K.K. and Pandey, A., Geoinformatics based assessment of coastal multi-hazard vulnerability along the East Coast of India: *Spatial Information Research*, (2019).
 45. Bathrellos, G., Skilodimou, H., Chousianitis, K., Youssef, A. and Pradhan, B., Suitability estimation for urban development using multi-hazard assessment map: *Science of The Total Environment*, (2017) 119–134.
 46. Skilodimou, H., Bathrellos, G., Chousianitis, K., Youssef, A. and Pradhan, B., Multi-hazard assessment modeling via multi-criteria analysis and GIS: a case study: *Environmental Earth Sciences*, 78 (2019).
 47. Bani-Mustafa, T., Zeng, Z., Zio, E. and Vasseur, D., A framework for multi-hazards risk aggregation considering risk model maturity levels. *IEEE; 2nd International Conference on System Reliability and Safety (ICSRS)*, Milan, Italy, 2017, pp. 429-433.
 48. Furlan, E., Torresan, S., Critto, A. and Marcomini, A., Spatially explicit risk approach for multi-hazard assessment and management in marine environment: The case study of the Adriatic Sea: *Science of the Total Environment*, 618 (2017).
 49. Mukhopadhyay, A., Hazra, S., Mitra, D. et al., Characterizing the multi-risk with respect to plausible natural hazards in the Balasore coast, Odisha, India: a multi-criteria analysis (MCA) appraisal: *Natural Hazards*, 80 (2016) 1495-1513.
 50. Chen, L., van Westen, C. J., Hussin, H., Ciurean, R. L., Turkington, T., Chavarro-Rincon, D. and Shrestha, D. P., Integrating expert opinion with modelling for quantitative multi-hazard risk assessment in the Eastern Italian Alps: *Geomorphology*, 273 (2016) 150–167.
 51. Ehlen, M. and Vargas, V., Multi-hazard, multi-infrastructure, economic scenario analysis: *Environment Systems & Decisions*, 33 (2013).
 52. Zhou, Y., Liu, Y., Wu, W. and Li, Ning., Integrated risk assessment of multi-hazards in China: *Natural Hazards*, 78 (2015).

53. Tian, C., Yiping, F., Yang, L. and Zhang, C., Spatial-temporal analysis of community resilience to multi-hazards in the Anning River basin, Southwest China: *International Journal of Disaster Risk Reduction*, 39 (2019).
54. Gill, J. and Malamud, B., Anthropogenic processes, natural hazards, and interactions in a multi-hazard framework: *Earth-Science Reviews*, 166 (2017).
55. Gallina, V., Torresan, S., Critto, A., Sperotto, A., Glade, T. and Marcomini, A., A review of multi-risk methodologies for natural hazards: Consequences and challenges for a climate change impact assessment: *Journal of Environmental Management*, 168 (2015) 123-132.
56. Barrantes, G., Multi-hazard model for developing countries: *Natural Hazards*, 92 (2018).
57. Liu, B., Siu, Y. L. and Mitchell, G., A quantitative model for estimating risk from multiple interacting natural hazards: an application to northeast Zhejiang, China: *Stochastic Environmental Research and Risk Assessment*. (2016).
58. Bernal, G., Salgado-Gálvez, M., Zuloaga Romero, D., Tristancho, J., González, D. and Cardona, O., Integration of Probabilistic and Multi-Hazard Risk Assessment Within Urban Development Planning and Emergency Preparedness and Response: Application to Manizales, Colombia: *International Journal of Disaster Risk Science*, 8 (2017).
59. Micu, M., Jurchescu, M., Micu, D., Zarea, R., Zumpano, V. and Bălteanu, D., A morphogenetic insight into a multi-hazard analysis: Bâsca Mare landslide dam: *Landslides*, 11 (2014).
60. Tilloy, A., Malamud, B., Winter, H. and Joly-Laugel, A., A review of quantification methodologies for multi-hazard interrelationships: *Earth-Science Reviews*, 196 (2019).
61. Chang, S., Yip, J., and Tse, W., Effects of urban development on future multi-hazard risk: the case of Vancouver, Canada: *Natural Hazards*, 98 (2018).
62. Mafi Gholami, D., Zenner, E., Jaafari, A., Riyahi Bakhtyari, H. R. and Tien Bui, D., Multi-hazards vulnerability assessment of southern coasts of Iran: *Journal of Environmental Management*, 252 (2019).

63. Fell, R., Jordi, C., Christophe, B., Leonardo, C., Eric, L. and William, Z. S., Guidelines for Landslide Susceptibility, Hazard and Risk Zoning for Land Use Planning: *Engineering Geology*, 102(3–4) (2008) 85–98.
64. Jacobs, L., Maes, J., Mertens, K., Sekajugo, J., Thiery, W., Lipzig, N., Poesen, J., Kervyn, M. and Dewitte, O., Reconstruction of a flash flood event through a multi-hazard approach: focus on the Rwenzori Mountains, Uganda: *Natural Hazards*, 84 (2016).
65. Kappes, M., Papathoma-Köhle, M., and Keiler, M., Assessing physical vulnerability for multi-hazards using an indicator-based methodology: *Applied Geography*, 32 (2012) 577-590.
66. Omidvar, B. and Karimi, H., Multi-hazard failure probability analysis of gas pipelines for earthquake shaking, ground failure and fire following earthquake: *Natural Hazards*, 82 (2016).
67. Liu, K., Wang, M., Cao, Y., Zhu, W. and Yang, G., Susceptibility of existing and planned Chinese railway system subjected to rainfall-induced multi-hazards: *Transportation Research Part A: Policy and Practice*, 117 (2018) 214-226.
68. Mirzaei, G., Soltani, A., Soltani, M. and Darabi, M., An integrated data-mining and multi-criteria decision-making approach for hazard-based object ranking with a focus on landslides and floods: *Environmental Earth Sciences*, 77 (2018).
69. Sheikh, V., Kornejady, A. and Ownegh, M., Application of the Coupled TOPSIS-Mahalanobis Distance for Multi-Hazard-Based Management of the Target Districts of the Golestan Province, Iran: *Natural Hazards* (2019).
70. Pourghasemi, H. R., Gayen, A., Panahi, M., Rezaie, F. and Blaschke, T., Multi-hazard probability assessment and mapping in Iran: *Science of the Total Environment*, 692 (2019).
71. Araya-Munoz, D., Metzger, M., Stuart, N., Wilson, A. and Carvajal, D., A spatial fuzzy logic approach to urban multi-hazard impact assessment in Concepción, Chile: *Science of the total environment*, (2017).

72. Kappes, M.S., Keiler, M., von Elverfeldt, K. and Glade, T., Challenges of analyzing multi-hazard risk: a review: *Natural Hazards*, 64 (2012) 1925-1958.
73. Ankara Büyükşehir Belediyesi._<http://www.ankara.bel.tr> (Last Access: 7 May 2020).
74. Mamak Belediyesi. <http://www.mamak.bel.tr/> (Last Access: 7 May 2020).
75. TMMOB İnşaat Mühendisleri Odası Ankara Şubesi. http://ankara.imo.org.tr/genel/bizden_detay.php?kod=24309&tipi=3&sube=3 (Last Access: 7 May 2020).
76. Hürriyet Gazetesi. <https://www.hurriyet.com.tr/heyelan-sokaginda-gece-yarisi-panigi-27495701> (Last Access: 7 May 2020).
77. Jeoloji Mühendisleri Odası. Mamak İlçesi Cengizhan Mahallesiindeki Heyelan Olayının İncelenmesi, https://www.jmo.org.tr/resimler/ekler/8c31c8b6a4960e8_ek.pdf (Last Access: 7 May 2020).
78. ESA. Sentinel-2, <https://sentinel.esa.int/web/sentinel/missions/sentinel-2> (Last Access: 27 January 2019).
79. Akbaş, B., Akdeniz, N., Aksay, A., Altun, İ., Balcı, V., Bilginer, E., Bilgiç, T., Duru, M., Ercan, T., Gedik, İ., Günay, Y., Güven, İ.H., Hakyemez, H. Y., Konak, N., Papak, İ., Pehlivan, Ş., Sevin, M., Şenel, M., Tarhan, N., Turhan, N., Türkecan, A., Ulu, Ü., Uğuz, M.F., Yurtsever, A. ve diğerleri. Türkiye Jeoloji Haritası, Maden Tetkik ve Arama Genel Müdürlüğü Yayını, **2002**, <http://yerbilimleri.mta.gov.tr/> (Last Access: 20 July 2018).
80. Moore, I. D., Grayson, R. B. and Ladson, A. R., Digital terrain modelling: A review of hydrological, geomorphological, and biological applications: *Hydrological Processes*, 5(1) (1991) 3–30.
81. ESA. Sentinel-2 coverage map, <https://sentinel.esa.int/web/sentinel/user-guides/sentinel-2-msi/revisit-coverage> (Last Access: 27 January 2019).
82. Poursanidis, D. and Chrysoulakis, N., Remote Sensing, Natural Hazards and the Contribution of ESA Sentinels Missions: Remote Sensing Applications: *Society and Environment*, 6 (2017) 25-38.

83. Pourghasemi, H. R. and Kerle, N., Random forests and evidential belief function-based landslide susceptibility assessment in Western Mazandaran Province, Iran: *Environmental Earth Sciences*, 75 (2016).
84. Ayalew, L. and Yamagishi, H., The Application of GIS-Based Logistic Regression for Landslide Susceptibility Mapping in the Kakuda-Yahiko Mountains, Central Japan: *Geomorphology*, 65 (2005) 15-31.
85. SAGA GIS, www.saga-gis.org (Last Access: 20 July 2019).
86. Esri, <https://www.esri.com/> (Last Access: 20 July 2018).
87. Wilson, J. P. and Gallant, J. C., Digital terrain analysis: Terrain analysis: Principles and applications, 6(12) (2000) 1–27.
88. Valencia, J., Ortiz, V. and Martínez-Graña, A., A neural network model applied to landslide susceptibility analysis (Capitanejo, Colombia): *Geomatics, Natural Hazards and Risk*, (2018)
89. Gökceoglu, C. and Aksoy, H., Landslide susceptibility mapping of the slopes in the residual soils of the Mengen region (Turkey) by deterministic stability analyses and image processing techniques: *Engineering Geology*, 44(1-4) (1996) 147–161.
90. Budimir, M., Atkinson, P. and Lewis, H., Seismically induced landslide hazard and exposure modelling in Southern California based on the 1994 Northridge, California earthquake event: *Landslides*, 12 (2014) 1-16.
91. Rasyid, A. R., Bhandary, N. P. and Yatabe, R., Performance of frequency ratio and logistic regression model in creating GIS based landslides susceptibility map at Lompobattang Mountain, Indonesia: *Geoenvironmental Disasters*, 3(1) (2016).
92. Zakerinejad, R. and Maerker, M., An integrated assessment of soil erosion dynamics with special emphasis on gully erosion in the Mazayjan basin, southwestern Iran: *Natural Hazards*, 79(S1) (2015) 25–50.
93. Kakembo, V., Xanga, W. W. and Rowntree, K., Topographic thresholds in gully development on the hillslopes of communal areas in Ngqushwa Local Municipality, Eastern Cape, South Africa: *Geomorphology*, 110(3-4) (2009) 188–194.

94. Samia, J., Temme, A., Bregt, A., Wallinga, J., Guzzetti, F., Ardizzone, F. and Rossi, M., Characterization and quantification of path dependency in landslide susceptibility: *Geomorphology*, 292 (2017) 16–24.
95. Breiman, L., *Random Forests: Machine Learning*, 45 (2001) 5–32.
96. Belgiu, M. and Drăguț, L., Random forest in remote sensing: A review of applications and future directions: *ISPRS Journal of Photogrammetry and Remote Sensing*, 114 (2016) 24–31.
97. Stefanski, J., Mack, B. and Waske, O., Optimization of Object-Based Image Analysis With Random Forests for Land Cover Mapping: *IEEE Journal of Selected Topics in Applied Earth Observations and Remote Sensing*, 6(6) (2013) 2492–2504.
98. Yoo, C., Han, D., Im, J. and Bechtel, B., Comparison between convolutional neural networks and random forest for local climate zone classification in mega urban areas using Landsat images: *ISPRS Journal of Photogrammetry and Remote Sensing*, 157 (2019) 155–170.
99. Ma, L., Li, M., Ma, X., Cheng, L., Du, P. and Liu, Y., A review of supervised object-based land-cover image classification: *ISPRS Journal of Photogrammetry and Remote Sensing*, 130 (2017) 277–293.
100. Lim, J., Kim, K. and Jin, R., Tree Species Classification Using Hyperion and Sentinel-2 Data with Machine Learning in South Korea and China: *International Journal of Geo-Information*, 8 (2019) 150.
101. Guo, L., Chehata, N., Mallet, C. and Boukir, S., Relevance of airborne lidar and multispectral image data for urban scene classification using Random Forests: *ISPRS Journal of Photogrammetry and Remote Sensing*, 66(1) (2011) 56–66.
102. Stumpf, A. and Kerle, N., Object-oriented mapping of landslides using Random Forests: *Remote Sensing of Environment*, 115(10) (2011) 2564–2577.
103. Lee, S., Application of logistic regression model and its validation for landslide susceptibility mapping using GIS and remote sensing data: *International Journal of Remote Sensing*, 26(7) (2005) 1477–1491.

104. Duman, T. Y., Can, T., Gokceoglu, C., Nefeslioglu, H. A. and Sonmez, H., Application of logistic regression for landslide susceptibility zoning of Cekmece Area, Istanbul, Turkey: *Environmental Geology*, 51(2) (2006) 241–256.
105. Wang, H. B. and Sassa, K., Comparative evaluation of landslide susceptibility in Minamata area, Japan: *Environmental Geology*, 47(7) (2005) 956–966.
106. Bai, S.-B., Wang, J., Lü, G.-N., Zhou, P.-G., Hou, S.-S. and Xu, S.-N., GIS-based logistic regression for landslide susceptibility mapping of the Zhongxian segment in the Three Gorges area, China: *Geomorphology*, 115(1-2) (2010) 23–31.
107. Das, I., Sahoo, S., Van Westen, C., Stein, A. and Hack, R., Landslide susceptibility assessment using logistic regression and its comparison with a rock mass classification system, along a road section in the northern Himalayas (India): *Geomorphology*, 114(4) (2010) 627–637.
108. Nefeslioglu, H.A. and Gokceoglu, C., Probabilistic risk assessment in medium scale for rainfall-induced earthflows: Catakli catchment area (Cayeli, Rize, Turkey): *Math. Probl. Eng* 2011, (2011).
109. Lee, S. and Pradhan, B., Landslide hazard mapping at Selangor, Malaysia using frequency ratio and logistic regression models: *Landslides*, 4(1) (2006) 33–41.
110. Vorpahl, P., Elsenbeer, H., Märker, M. and Schröder, B., How can statistical models help to determine driving factors of landslides?: *Ecological Modelling*, 239 (2012) 27–39.
111. Park, S., Choi, C., Kim, B. and Kim, J., Landslide susceptibility mapping using frequency ratio, analytic hierarchy process, logistic regression, and artificial neural network methods at the Inje area, Korea: *Environmental Earth Sciences*, 68(5) (2012) 1443–1464.
112. Mamdani, E.H. and Assilian, S., Experiment in linguistic synthesis with a fuzzy logic controller: *International Journal of Man-Machine Studies*, 7(1) (1975) 1-13.
113. Zadeh, L. A., *Fuzzy Sets: Inf. Control*, 8(3) (1965) 338-353.

114. Grima, M. A., Neuro-Fuzzy Modeling in Engineering Geology. A.A. Balkema, Rotterdam, (2000) 244.
115. Gokceoglu, C. and Zorlu K., A fuzzy model to predict the uniaxial compressive strength and the modulus of elasticity of a problematic rock: Engineering Applications of Artificial Intelligence, 17 (1) (2004) 61-72.
116. Akgun, A., Sezer, E. A., Nefeslioglu, H. A., Gokceoglu, C. and Pradhan, B., An easy-to-use MATLAB program (MamLand) for the assessment of landslide susceptibility using a Mamdani fuzzy algorithm: Computers & Geosciences, 38(1) (2012) 23–34.
117. Osna, T., Sezer, E.A. and Akgun, A., GeofIS: An integrated tool for the assessment of landslide susceptibility: Computers & Geosciences, 66 (2014) 20-30.
118. Sezer, E.A., Nefeslioglu, H.A. and Osna, T., An expert-based landslide susceptibility mapping (LSM) module developed for Netcad Architect Software: Computers and Geosciences, 98 (2017) 26-37.
119. Ozer, B.C., Mutlu, B., Nefeslioglu, H., Sezer, E., Rouai, M., Dekayir, A. and Gokceoglu, C., On the use of hierarchical fuzzy inference systems (HFIS) in expert-based landslide susceptibility mapping: the central part of the Rif Mountains (Morocco): Bulletin of Engineering Geology and the Environment, 79 (2020) 551–568.
120. Zadeh, L.A., A Rationale for Fuzzy Control: Journal of Dynamic Systems, Measurement and Control Transaction ASME, 94 (1972) 3–4.
121. Hadipriono, F. and Sun, K., Angular Fuzzy Set Models for Linguistic Values: Civil Engineering Systems, 7(3) (1990) 148–156.
122. Karr, C.L. and Gentry, E.J., Fuzzy Control of pH Using Genetic Algorithms: IEEE Transaction on Fuzzy Systems, 1(1) (1993) 46–53.
123. Perlich, C., Provost, F. and Simonoff, J., Tree Induction vs. Logistic Regression: A Learning-Curve Analysis: Journal of Machine Learning Research, 4 (2003) 211-255.

124. Van Westen, C. J., Van Asch, T. W. J. and Soeters, R., Landslide hazard and risk zonation—why is it still so difficult? : Bulletin of Engineering Geology and the Environment, 65(2) (2005) 167–184.
125. Endeksa, Ankara, Mamak, <https://www.endeksa.com/tr/analiz/ankara/mamak/demografi#gelir> (Last Access: 03 April 2020)
126. Göközkut B. and Somuncu M., Ankara’da Yeni Mamak Kentsel Dönüşüm Projesi Ölçeğinde Dönüşen Mekânlar, Değişen Gündelik Hayat Pratikleri: Ankara Araştırmaları Dergisi, 7(1) (2019) 105-124.
127. Mamak Belediyesi. Mamak Belediyesi 2018 Yılı İdare Faaliyet Raporu., <https://www.mamak.bel.tr/wp-content/uploads/2017/03/2018-faaliyet.pdf> (Last Access: 20 July 2019)
128. Cutter, S. L., The landscape of disaster resilience indicators in the USA: Natural Hazards, 80(2) (2015) 741–758.
129. QT Modeller, <http://appliedimagery.com/> (Last Access: 29 December 2019)
130. Özmen, B. and Özden, A., Türkiye'nin Afet Yönetim Sistemine İlişkin Eleştirel Bir Değerlendirme, A Critical Evaluation Related To Disaster Management System Of Turkey. İstanbul Üniversitesi Siyasal Bilgiler Fakültesi Dergisi, 2013.
131. Balamir, M., Painful Steps of Progress from Crisis Planning to Contingency Planning: Changes for Disaster Preparedness in Turkey: Journal of Contingencies and Crisis Management, 10(1) (2002) 39–49.
132. Şenol Balaban, M., Hazard-Prone Cities and Recent Challenges in the Case of Urban Transformation Experience of Turkey. Urban and Regional Planning in Turkey, (2019) 235–259.
133. Balamir, M., Reproducing the Fatalist Society: An Evaluation of the Disasters and Development Laws and Regulations in Turkey', in Urban Settlements and Natural Disasters, ed. E. Komut: International Union of Architects and Chamber of Architects of Turkey, (1999) 96-107.
134. Balamir, M., Afet Politikası, Risk ve Planlama: TMMOB Afet Sempozyumu Bildiriler Kitabı, Ankara, (2007) 31-43.

135. Barría, P., Cruzat, M. L., Cienfuegos, R., Gironás, J., Escauriaza, C., Bonilla, C., ... Torres, A., From Multi-Risk Evaluation to Resilience Planning: The Case of Central Chilean Coastal Cities: *Water*, 11(3) (2019) 572.



APPENDIX

APPENDIX 1 - Publications derived from the thesis

- Yanar, T., Kocaman, S. and Gokceoglu, C., Use of Mamdani Fuzzy Algorithm for Multi-Hazard Susceptibility Assessment in a Developing Urban Settlement (Mamak, Ankara, Turkey): ISPRS International Journal of Geo-Information, 9 (2020) 114. 10.3390/ijgi9020114.



APPENDIX 2 - Proceedings derived from thesis

- Yanar, T., Kocaman, S. and Gokceoglu, C., On the Use of Sentinel-2 Images and High Resolution DTM for Landslide Susceptibility Mapping in a Developing Urban Settlement (Mamak, Ankara, Turkey). In International Archives of the Photogrammetry, Remote Sensing & Spatial Information Sciences, Proceedings of the Geoinformation for Disaster Management (Gi4DM), Prague, Czech Republic, 3–6 September 2019; ISPRS: Hannover, Germany, 2019; Volume XLII-3/W8, **2019**, pp. 469–476. 10.5194/isprs-archives-XLII-3-W8-469-2019.



APPENDIX 3 - Thesis Originality Report



HACETTEPE UNIVERSITY
GRADUATE SCHOOL OF SCIENCE AND ENGINEERING
THESIS/DISSERTATION ORIGINALITY REPORT

HACETTEPE UNIVERSITY
GRADUATE SCHOOL OF SCIENCE AND ENGINEERING
TO THE DEPARTMENT OF GEOMATICS ENGINEERING

Date: 13/05/2020

Thesis Title / Topic: Multi-Hazard Susceptibility Map Production For Urban Planning Purposes: Ankara Mamak Case

According to the originality report obtained by myself/my thesis advisor by using the *Turnitin* plagiarism detection software and by applying the filtering options stated below on 13/05/2020 for the total of 53 pages including the a) Title Page, b) Introduction, c) Main Chapters, d) Conclusion sections of my thesis entitled as above, the similarity index of my thesis is 6%.

Filtering options applied:

1. Bibliography/Works Cited excluded
2. Quotes excluded / included
3. Match size up to 5 words excluded

I declare that I have carefully read Hacettepe University Graduate School of Science and Engineering Guidelines for Obtaining and Using Thesis Originality Reports; that according to the maximum similarity index values specified in the Guidelines, my thesis does not include any form of plagiarism; that in any future detection of possible infringement of the regulations I accept all legal responsibility; and that all the information I have provided is correct to the best of my knowledge.

I respectfully submit this for approval.

Date and Signature

Name Surname: Tuğçe YANAR
Student No: N18130611
Department: Geomatics Engineering
Program: Geomatics Engineering
Status: Masters Ph.D. Integrated Ph.D.

13.05.2020
T.YANAR

ADVISOR APPROVAL

APPROVED.

Assoc. Prof. Dr. Sultan KOCAMAN GÖKÇEOĞLU

CURRICULUM VITAE

Name Surname : Tuğçe Yanar
Place of Birth : Altındağ
Date of Birth : 25.11.1995
Marital Status : Single
Address : Osmangazi Mahallesi, Zeytinbeli Sokak 6/13
Keçiören/ANKARA
Phone : 0505 883 87 74
E-mail : yanar.tugce@gmail.com
Foreign Language : English

EDUCATION STATUS

Bsc. : Middle East Technical University – City and Regional
Planning
Msc. : -
PhD. : -

WORK EXPERIENCE

16/07/2019–06/12/2019 : ESRI Turkey, Ankara (Turkey)
05/11/2018–15/05/2020 : Scholarship Holder (TUBİTAK), Ankara (Turkey)
01/04/2018–01/09/2018 : Project Worker - Assoc. Prof. Dr. Jan Bertram and Assoc.
Prof. Dr. G. Ilgezdi Bertram's Central Anatolian Early Bronze Age Project, Ankara
(Turkey)
07/08/2017–30/08/2017 : Başarsoft Information Technologies Inc., Ankara (Turkey)
03/07/2017–28/07/2017 : Municipality of Keçiören, Ankara (Turkey)

Other

International Certificates: ArcGIS Desktop Associate 19-001 Certificate